UNITED STATES DEPARTMENT OF COMMERCE

Maurice H. Stans, *Secretary*

NATIONAL BUREAU OF STANDARDS • A. V. Astin, *Director*

Thermodynamic Properties of Argon From the Triple Point to 300 K at Pressures to 1000 Atmospheres

A. L. Gosman,* R. D. McCarty,** and J. G. Hust**

*Wichita State University, Wichita, Kansas, and
Cryogenics Division
Institute for Basic Standards
National Bureau of Standards
Boulder, Colorado 80302

**Cryogenics Division
Institute for Basic Standards
National Bureau of Standards
Boulder, Colorado 80302

NSRDS–NBS 27

National Standard Reference Data Series-
National Bureau of Standards 27

Issued March 1969

For sale by the Superintendent of Documents, U.S. Government Printing Office
Washington, D.C. 20402 - Price $1.25

Library of Congress Catalog Card Number: 68-62109

Foreword

The National Standard Reference Data System is a Government-wide effort to provide for the technical community of the United States effective access to the quantitative data of physical science, critically evaluated and compiled for convenience, and readily accessible through a variety of distribution channels. The System was established in 1963 by action of the President's Office of Science and Technology and the Federal Council for Science and Technology.

The responsibility to administer the System was assigned to the National Bureau of Standards and an Office of Standard Reference Data was set up at the Bureau for this purpose. Since 1963, this Office has developed systematic plans for meeting high-priority needs for reliable reference data. It has undertaken to coordinate and integrate existing data evaluation and compilation activities (primarily those under sponsorship of Federal agencies) into a comprehensive program, supplementing and expanding technical coverage when necessary, establishing and maintaining standards for the output of the participating groups, and providing mechanisms for the dissemination of the output as required.

The System now comprises a complex of data centers and other activities, carried on in Government agencies, academic institutions, and nongovernmental laboratories. The independent operational status of existing critical data projects is maintained and encouraged. Data centers that are components of the NSRDS produce compilations of critically evaluated data, critical reviews of the state of quantitative knowledge in specialized areas, and computations of useful functions derived from standard reference data. In addition, the centers and projects establish criteria for evaluation and compilation of data and make recommendations on needed modifications or extensions of experimental techniques.

Data publications of the NSRDS take a variety of physical forms, including books, pamphlets, loose-leaf sheets and computer tapes. While most of the compilations have been issued by the Government Printing Office, several have appeared in scientific journals. Under some circumstances, private publishing houses are regarded as appropriate primary dissemination mechanisms.

The technical scope of the NSRDS is indicated by the principal categories of data compilation projects now active or being planned: nuclear properties, atomic and molecular properties, solid state properties, thermodynamic and transport properties, chemical kinetics, colloid and surface properties, and mechanical properties.

An important aspect of the NSRDS is the advice and planning assistance which the National Research Council of the National Academy of Sciences–National Academy of Engineering provides. These services are organized under an overall Review Committee which considers the program as a whole and makes recommendations on policy, long-term planning, and international collaboration. Advisory Panels, each concerned with a single technical area, meet regularly to examine major portions of the program, assign relative priorities, and identify specific key problems in need of further attention. For selected specific topics, the Advisory Panels sponsor subpanels which make detailed studies of users' needs, the present state of knowledge, and existing data resources as a basis for recommending one or more data compilation activities. This assembly of advisory services contributes greatly to the guidance of NSRDS activities.

The NSRDS–NBS series of publications is intended primarily to include evaluated reference data and critical reviews of long-term interest to the scientific and technical community.

A. V. ASTIN, *Director.*

Contents

List of Figures

List of Tables

Nomenclature, Conversions, Physical Constants, and Fixed Points for Argon

Nomenclature

P – absolute pressure
T – absolute temperature
V – specific volume
ρ – density $= 1/V$
R – universal gas constant
Z – compressibility factor $= PV/RT$
U – specific internal energy
H – specific enthalpy
S – specific entropy
C_p – specific heat capacity at constant pressure
C_v – specific heat capacity at constant volume
μ – Joule-Thomson coefficient
B – second virial coefficient
G – Gibbs function
A – Helmholtz function
$\bar{A}$ – residual work content
E – potential energy
r – distance of molecular separation
σ – molecular separation for $E = 0$
ϵ – Maximum energy of attraction
k – Boltzmann constant
N – Avogadro constant
r^* – reduced distance $= r/\sigma$
T^* – reduced temperature $= kT/\epsilon$
b_0 – reducing parameter $= 2\pi N\sigma^3/3$
B^* – reduced second virial coefficient $= B/b_0$
ρ_0 – distance between cores for minimum energy
h – Planck constant
a – radius of core
m – mass of molecule
$\bar{\Lambda}^*$ – de Broglie wave length $= h/(\sigma\sqrt{m\epsilon})$

Superscripts:
o – ideal gas property
$*$ – real or ideal gas property at very low pressures (P approaching 0) except as noted in symbols above
l – saturated liquid property
g – saturated vapor property

Subscripts:
c – critical point
o – reference state property
sat – property at saturation
t – triple point
expr – experimentally determined property value
calc – calculated property value
melt – melting line property

Subscripts on partial derivatives and integrals indicate which property is being held constant.

Conversions and Physical Constants

1 thermochemical calorie = 4.184 joules
0° C = 273.15 K (Triple point of water = 273.16 K)
Gas constant, $R = 0.0820535$ liter-atm/g-mole K
Planck constant, $h = 6.6256 \times 10^{-34}$ joule-sec
Boltzmann constant, $k = 1.38054 \times 10^{-23}$ joule/K
Avogadro constant, $N = 6.02252 \times 10^{23}$ per mole
Molecular weight of argon = 39.948g/g-mole (based on the carbon-12 scale where the isotope $C^{12} = 12.000\ldots$).

Fixed Points for Argon

Critical pressure = 48.34* atmospheres
Critical density = 300.4* Amagat = 13.41 g-mole/liter
Critical temperature = 150.86* K
Normal boiling point = 87.280 ± 0.015** K
Triple point temperature = 83.80** K
Triple point pressure = 0.68005** atmospheres.

* These fixed points are those listed by Michels et al. [1]. Some recent investigations indicate the critical temperature and pressure may be in error. However, these values appear to be the best estimate available at this writing. In reference [1] the Amagat unit of density is given as 4.4647×10^{-5} moles/cm³, based on the chemical scale. In this work the physical scale is used, resulting in an Amagat density unit of 4.4659×10^{-5} moles/cm³.

** These fixed points are those listed by Ziegler et al. [2]. The value of the normal boiling point calculated by the vapor pressure equation developed in this work agrees with that listed by Ziegler [2]. The value of the triple point temperature calculated by the vapor pressure equation developed in this work deviates from Ziegler's reported value by 0.0045 percent.

Thermodynamic Properties of Argon from the Triple Point to 300 K at Pressures to 1000 Atmospheres

A. L. Gosman, R. D. McCarty, and J. G. Hust

Tabular values of density, internal energy, enthalpy, and entropy of liquid and gaseous argon are presented for temperatures from 83.8 to 300 K at pressures of 0.01 to 1000 atmospheres. Diagrams of specific heats, compressibility factor, and entropy are included. The properties presented are calculated from an equation of state which was fitted to experimental P–ρ–T data from the world literature. Extensive comparisons were made between the equation of state and the experimental data, and deviation plots are presented. The second virial coefficient and Joule-Thomson inversion curve were also calculated and comparisons made with values from other sources. A vapor pressure equation which covers the range from the triple point to the critical point is also given.

Key Words: Argon; compressibility factor; enthalpy; entropy; equation of state; internal energy; Joule-Thomson coefficient; P–V–T; specific heat; vapor pressure; virial coefficient.

1. Introduction

In recent years technical interest in pure argon has greatly accelerated. This accelerated interest has been evidenced by a demand which has more than sextupled in 12 years. United States production has continued to increase from less than 200,000,000 cubic feet per year in 1953 to almost 1,300,000,000 cubic feet in 1965, with about 80 percent being shipped in liquid form [3].[1]

In addition, scientific interest in argon has arisen because of its characteristically "ideal" structural makeup. That is, argon is monatomic, with the relatively uncomplicated interatomic forces being approximated by spherically symmetric, nonpolar models. In addition, the quantum effects on argon are relatively small. Although helium and neon might be considered to be more "ideal" fluids from the standpoint of simple models, the quantum effects are relatively large for these two fluids as compared to argon. For these reasons argon might be expected to permit a more direct classical investigation and experimental verification of the theoretical model predictions.

In view of the increased activity in cryogenic engineering and physics, it was apparent that a set of consistent thermodynamic properties, over a relatively large region of the thermodynamic surface, was needed. Although many investigators had published data for the thermodynamic properties of argon, each tabulation was, in general, limited to the property range of interest of the specific investigator, and large gaps in the data existed. In addition, where the ranges of data did overlap, there was a substantial degree of inconsistency in some instances. For these reasons, this laboratory undertook the program of making a critical analysis of the thermodynamic properties of argon in the cryogenic temperature range, including the low temperature–high density region.

In recent years, much of the technical design and synthesis has been done with the aid of high speed digital computers. Thus the need for an analytical equation of state has become quite significant when compared with the use of tables and charts of thermodynamic properties. Many equations of state have been proposed in the literature, each with its own peculiar strengths and weaknesses. Some of these equations represented the data in certain regions of the thermodynamic surface, but were quite inadequate in other regions of the surface. Therefore, the need was established for a single equation of state which could accurately and consistently represent the data for both the liquid and vapor phases with a consistent transition from the low temperature–high density region to the low density region.

In the case of argon, it is difficult to assess the general overall adequacy of an equation of state in terms of deviations from the experimental P-V-T surface. That is, due to the inconsistency of some of the overlapping experimental data sources, there is no single experimental P-V-T surface which can be used as a reference. Also, the significance of the deviations is wholly dependent upon the variable chosen for the comparison and the specific region of the thermodynamic surface which is being studied. In certain regions of the surface,

[1] Figures in brackets indicate the literature references (sec. 17).

large pressure deviations are caused by insignificant density errors, while in other regions the reverse is true. In general, the equation of state presented in section 7 represents the different sources of experimental data to within the accuracy of the data, except at the higher temperatures on the coexistence boundary and the critical region where the deviations are, in a few cases, greater than the accuracy of the data. Numerous deviation plots are presented (sec. 8) in a manner which permits the comparison of the equation of state with each of the experimental data sources over the various regions of the thermodynamic surface.

As a part of the critical analysis, it was deemed necessary to develop a vapor pressure equation which would accurately represent the experimental vapor pressure data from the triple point to the critical point. This vapor pressure equation could then be used, in conjunction with the equation of state, to calculate some of the derived thermodynamic properties such as enthalpy, entropy, etc.

Thus it was concluded that a critical analysis of thermodynamic properties of argon was to be made for temperatures to about 300 K and for pressures to about 1000 atm wherever the experimental data permitted this pressure range.

2. Survey of the Literature

A comprehensive search of the literature resulted in a bibliography of about 425 references. The temperatures which were included in this search covered the range from 0 to 300 K. In addition to manual-reviewing techniques, the data retrieval personnel and the computerized search techniques of the Cryogenic Data Center of the National Bureau of Standards at Boulder, Colo. were utilized. As a result, a bibliography on the thermophysical properties of argon [4] was prepared and published in 1964. The literature search was continually updated so that current data were rapidly assimilated.

From this literature search, the most appropriate *P-V-T* data, vapor pressure data, coexistence density data, and fixed point data were selected for consideration and evaluation. In addition, virial coefficient data, Joule-Thomson data, specific heat data, and information on equations of state were acquired and considered.

Although many equations of state were presented in the literature, none of these equations appeared to have been developed to adequately represent the data for argon for temperatures from below the normal boiling point to twice the critical temperature for the gaseous, dense gas, and liquid regions. Hirschfelder et al. [5] developed a generalized equation of state which arbitrarily divided the *P-V-T* surface into three regions, namely, gas, dense gas, and liquid regions. For these three regions, Hirschfelder et al. [5] developed three equations in such a manner that discontinuities at the junction of these regions were avoided.

Appearing in the literature were other techniques for representing the *P-V-T* data. For some fluids, where perhaps one source of highly precise data were available, the *P-V-T* data could be represented by polynomials along isotherms or polynomials along isochores. One such isothermal representation is the virial equation of state.

The virial equation of state is based on fundamental grounds in that it can be derived from fundamental statistical mechanics. Furthermore, in principle, this equation of state depends upon a very small number of parameters in that once one characterizes the potential function (by assigning values to its parameters) all virial coefficients can be calculated. In practice, however, only the second virial coefficient has been calculated properly. The third virial has been calculated in the approximation where nonadditivity is neglected for a small number of functions. All higher virials have really not been calculated except for the fourth and fifth virials for the hard sphere and (12–6) potentials. Thus, in actual practice, a virial equation of state is, in effect, an equation of state with a number of parameters equal to the number of virials times the number of isotherms (perhaps minus the second virials). Thus, Michels et al. [1, 6] equation of state remains a 100 parameter representation of his 19 isotherms until higher virials can be properly calculated from potential functions.

In addition, where multiple sets of data exist (as with argon) at odd temperature and density spacings, a complete correlation at all points of the *P-V-T* surface becomes very difficult with these polynomials. That is, if isothermal polynomials are used, then each set of coefficients is valid only for the one specific isotherm which was fitted. If a point on the *P-V-T* surface lies between two of the fitted isotherms, then other interpolative techniques must be used to obtain the *P-V-T* coordinates of this point.

3. Summary of *P-V-T* Data

Published experimental *P-V-T* data were reviewed and examined. As a result, the *P-V-T* data which were considered for use in this compilation were distributed as shown in table 1.

Evaluation of the experimental *P-V-T* data of van Itterbeek, Verbeke, and Staes [9] revealed slight inconsistencies. Private communication from Verbeke [12] indicated that there were typographical errors in the original paper [9]. The new values given by Verbeke [12] were then used in this work.

TABLE 1. *Summary of* P-V-T *data*

Number of points	Temperature or volume	Pressure range (atm)	Source
8	−140 °C	6 to 160	Michels, Levelt, and de Graaff [1]
10	−135	7 to 200	[1]
13	−130	7 to 240	[1]
17	−125	7 to 280	[1]
20	−122.5	7 to 300	[1]
24	−120	7 to 320	[1]
26	−110	8 to 400	[1]
26	−100	8 to 480	[1]
26	−85	9 to 600	[1]
27	−70	6 to 700	[1]
27	−50	7 to 850	[1]
28	−25	7 to 1030	[1]
41	Near coexistence region		[1]
48	0 °C	19 to 930	Michels, Wijker, and Wijker [6]
46	25	20 to 870	[6]
15	50 to 150 °C	27 to 750	[6]
7	−183.02 °C	26 to 165	Rogovaya and Kaganer [7]
8	−150.08	25 to 185	[7]
6	−135.03	72 to 196	[7]
6	−120.02	73 to 166	[7]
7	−110.04	47 to 176	[7]
9	−100.01	49 to 192	[7]
7	−90.03	50 to 190	[7]
8	−75.03	26 to 194	[7]
8	−49.93	28 to 197	[7]
8	−24.98	27 to 184	[7]
8	86.63 K	17 to 90	van Itterbeek and Verbeke [8]
14	87.91	13 to 147	[8]
14	89.13	22 to 150	[8]
14	90.55	18 to 146	[8]
8	90.15 K	10 to 242	van Itterbeek, Verbeke, and Staes [9]
12	96.99	11 to 280	[9]
12	108.18	19 to 260	[9]
8	117.10	16 to 284	[9]
7	127.05	30 to 290	[9]
7	130.85	21 to 266	[9]
11	134.40	30 to 258	[9]
16	136.02	40 to 257	[9]
14	138.98	33 to 285	[9]
11	146.63	58 to 248	[9]
9	148.25	45 to 288	[9]

TABLE 1. *Summary of* P-V-T *data*—Continued

Number of points	Temperature or volume	Pressure range (atm)	Source
1	93.15 K	320	van Witzenburg [10]
5	98.15	78 to 350	[10]
7	103.15	76 to 330	[10]
12	123.15	303 to 1042	[10]
12	128.15	302 to 1908	[10]
15	133.15	207 to 1941	[10]
7	108.15	322 to 1210	[10]
3	113.15	74 to 967	[10]
10	118.15	296 to 1590	[10]
13	138.15	315 to 1957	[10]
16	148.15	66 to 1902	[10]
13	153.15	315 to 1925	[10]
14	29.2 cm^3/g-mol	21 to 488	Walker [11]
15	29.6	25 to 494	[11]
17	29.8	43 to 520	[11]
20	31.3	39 to 500	[11]
17	33.8	16 to 515	[11]
24	35.7	24 to 500	[11]
22	37.8	27 to 506	[11]
16	39.5	34 to 286	[11]
16	41.2	34 to 483	[11]
23	42.0	38 to 506	[11]
24	43.6	45 to 316	[11]
25	45.5	43 to 272	[11]
14	50.7	45 to 139	[11]
22	58.3	61 to 209	[11]
13	66.5	45 to 122	[11]

A preliminary comparison of Walker's [11] experimental data showed an inconsistency in the published density values. Private communication from Walker [13] indicated that there were errors in the density values quoted in the original paper [11]. A more complete discussion of Walker's [11] data will be given later.

4. Summary of Vapor Pressure Data

Some of the vapor pressure data which are available in the literature were published in the early part of the century. Wherever possible, these early data were replaced by more recent data if there appeared to be sufficient evidence that the recent data were of higher reliability.

Modern experimental instrumentation and techniques generally permit a higher order of accuracy and precision than did the earlier work. In addition, the temperature scales and basic standards which were used in much of the older work were substantially different from those used today. Some of the earlier work may have been conducted with variations in the temperature scales of as much as 0.06 deg. Much of the time, the early investigator did not clearly state which temperature scale was in current use and the results therefore lead to confusion and uncertainty.

As a result of the above considerations, the vapor pressure data which were selected for further analysis are shown in table 2.

In addition to the vapor pressure data shown above, two sources of coexistence or saturation densities were examined. These are indicated in table 3.

TABLE 2. *Summary of vapor pressure data*

Number of points	Temperature range—K	Source
23	90 to 150	van der Waals Laboratory data reported by Clark, Din, Robb, Michels, Wassenaar, and Zwietering [14].
17	86 to 150	British Oxygen Co. Ltd. data reported by Clark et al. [14].
23	117 to 150	Michels, Levelt, and de Graaff [1].
6	84 to 87	Flubacher, Leadbetter, and Morrison [15].
34	85 to 148	van Itterbeek, de Boelpaep, Verbeke, Theeuwes, and Staes [16].
9	129 to 147	van Itterbeek, Verbeke, and Staes [9].

TABLE 3. *Coexistence density data*

Number of points	Temperature range—K	Source
23	117–150	Michels, Levelt, and de Graaff [1].
16	90–148	Mathias, Onnes, and Crommelin [17].

5. Saturated Liquid Density

In this analysis, it frequently was found convenient to have an expression which could be used to predict approximate values for the density of the saturated liquid. This type of expression was not needed for the determination of the equation of state or the calculation of the thermodynamic properties. However, it would prove useful in the preliminary analysis, where saturation data were evaluated for consistency. Such an expression also would be useful for obtaining initial approximations in iterative solutions of the equation of state. For these purposes a simple expression, based upon the principle of corresponding states, was developed.

Using the critical point as the reducing parameter, the principle of corresponding states assumes a universal function which may be expressed as

$$P_r = f(T_r, V_r) \tag{1}$$

where

$$P_r = P/P_c$$
$$T_r = T/T_c$$
$$V_r = V/V_c.$$

However, in the coexistence region where the saturated liquid and saturated vapor are in mutual equilibrium, the pressure and temperature are not independent properties. Thus if eq (1) were examined in accordance with the thermodynamic requirements of the coexistence line, it may be deduced that there also exists a universal function for the saturated liquid such that

$$\rho^l/\rho_c = F(T_r). \tag{2}$$

Using a coordinate system of reduced temperature versus reduced density, Guggenheim [18] plotted experimental data points for a number of pure substances and verified the universal form of eq (2). For the data which Guggenheim [18] had available, he found that the coexistence line could be adequately expressed by the relationships

$$\frac{\rho^l + \rho^g}{2\rho_c} = 1 + a(1 - T_r) \tag{3}$$

and

$$\frac{\rho^l - \rho^g}{\rho_c} = b(1 - T_r)^{1/3}, \tag{4}$$

where a and b are constants. Equation (3) represents the "law" of the rectilinear diameter which states that the average of the saturated liquid and saturated vapor densities appears as a straight line on the reduced coordinate system of temperature versus density.

Combining eqs (3) and (4) yields an equation for the saturated liquid density, expressed as

$$\rho^l/\rho_c = 1 + a(1 - T_r) + C(1 - T_r)^{1/3} \tag{5}$$

where $C = b/2$.

In order to represent the data with more accuracy than eq (5) permits, an expanded form of eq (5) was proposed. Physical requirements demand that the derivative

$$\frac{d(T_r)}{d(\rho^l/\rho_c)} = 0 \text{ at } \rho^l = \rho_c, \text{ and } T_r = 1 \tag{6}$$

Thus the possibility of an equation with the saturated liquid density as a function of only integer powers of temperature is ruled out, since such an equation would not fulfill the requirements of eq (6). It then appears that a fractional power term such as the last term in eq (5) is necessary so that zero slope may exist at the critical point. An expanded form of eq (5) may then be written as

$$\rho^l/\rho_c = \sum_{n=0,\,1,\,2,\,3,\,\ldots} d_n (1 - T_r)^{n/3}. \tag{7}$$

For eq (7) to satisfy critical point behavior, the coefficient d_0 should be essentially equal to unity. In addition, if the derivative of eq (7) is written

$$\frac{d(T_r)}{d(\rho^l/\rho_c)} = -\frac{1}{\sum_{n=0,\,1,\,2,\,3,\,\ldots} \frac{n}{3} d_n (1 - T_r)^{\frac{n}{3} - 1}}, \tag{8}$$

it is seen that the requirements of eq (6) are satisfied. In eq (7), fractional exponents other than multiples of 1/3 were investigated. The results showed no apparent advantages, and the 1/3 exponent was retained.

Equation (7) was fitted to the saturated liquid data by least square techniques. A series of successive fits was performed with increasing values of "n." Examination of these fits revealed a continued decrease in the deviations between the calculated density and experimental density until the fit with $n = 6$. For fits with "n" greater than six, the results appeared to be approaching the precision of the data, and, therefore, the final form for the equation was selected to be

$$\rho^l/\rho_c = \sum_{n=0}^{6} d_n K^n \tag{9}$$

where $K = (1 - T_r)^{1/3}$ and T_r is calculated from temperatures in Kelvin units.

An examination of the saturated liquid density data demonstrates that the data from Michels et al. [1] and Mathias et al. [17] are consistent with each other, with Michels' data showing somewhat more precision. This may be seen in figure 1, where

percent density deviation is plotted as a function of temperature.

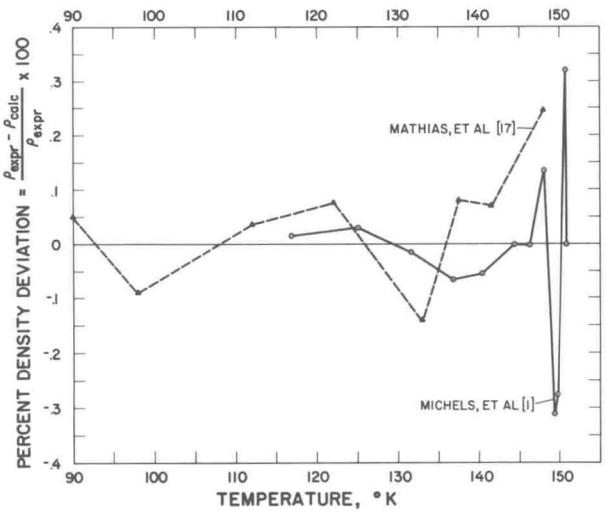

FIGURE 1. *Deviations between calculated (eq (9)) saturation liquid densities and experimental saturated liquid densities.*

In figure 1, it is seen that both sets of data exhibit almost the same characteristics with the Mathias data showing a wider envelope of density deviations. The maximum deviation of the saturated liquid density data from that calculated by eq (9) is 0.32 percent which occurs within 1/2 deg of the critical point. The mean of the absolute values of density deviations for Michels' data is 0.099 percent, and for the data of Mathias, 0.098 percent.

However, the three Michels' data points which exhibit the largest density deviations are all within about a degree and a half of the critical point where the experimental determination of saturated liquid densities becomes most difficult. If these three points are not included, then the mean density deviation is 0.039 percent. On the other hand, the single data point of the Mathias data which exhibits the maximum deviation is within about two and a half degrees of the critical point. If this point is omitted, the mean density deviation for the Mathias data is 0.076 percent.

With these comparisons, it can be concluded that eq (9) adequately represents the data, with precision approaching the precision of the data. In addition, the data of Michels et al. [1] display a precision about twice that of Mathias et al. [17].

The coefficients of eq (9) which resulted from the fit with $n=6$ are shown in table 4.

TABLE 4. *Coefficients for saturated liquid densities for eq (9)*

Temperature in K, coefficients are dimensionless	
$d_0 = 0.99995448$	$d_4 = 91.361470$
$d_1 = 0.47354891$	$d_5 = -93.773992$
$d_2 = 11.238328$	$d_6 = 37.769045$
$d_3 = -43.741090$	

Use of the coefficients in table 4 produces a root-mean-square deviation in ρ^l/ρ_c of 0.002 for the data considered.

6. Vapor Pressure

The purpose of developing a vapor pressure equation was twofold. When used in conjunction with an independently obtained equation of state, the vapor pressure equation could be used to define the coexistence boundary. Also, the vapor pressure equation could be used in conjunction with the equation of state to calculate some of the derived thermodynamic properties.

The coexistence boundary may also be defined without the use of a vapor pressure equation, as discussed in section 11. However, this method requires a sufficient number of highly precise experimental *P-V-T* data points along the boundary. Since saturation densities are difficult to measure with a high degree of precision, and since there was only one source of satisfactory coexistence data, it was difficult to perform a critical evaluation of this data for the purpose of establishing the coexistence boundary.

Instead, there was in the literature a relatively large number of experimental *P-T* data points along the coexistence boundary. With these data a vapor pressure equation could be developed. An examination of the literature indicated the existence of many vapor pressure equations which have been used. Some of these have been studied, compared, and listed by Stewart [19].

For this evaluation of argon, a vapor pressure equation was developed which would represent the argon data with sufficient precision and at the same time permit consistency with the equation of state at the critical point.

The argon vapor pressure equation was developed from the application of the Clapeyron equation to a first order phase transition. The Clapeyron equation is

$$\left(\frac{dP}{dT}\right)_{sat} = \frac{H^g - H^l}{T(V^g - V^l)}. \tag{10}$$

If appropriate expressions for the changes in enthalpy and volume as functions of temperature and pressure are substituted in eq (10), the equation can then be integrated to give the desired vapor pressure equation. Some of the simpler and more commonly used vapor pressure equations were obtained with the assumptions of

$$V^g \gg V^l;\ V^g = \frac{RT}{P};\ H^g - H^l = \text{constant}. \tag{11}$$

The first assumption of eq (11) is valid only for coexistence states which are considerably below the critical point. In addition, figures 2 and 3 illustrate that the second and third assumptions of eq (11) are in substantial error.

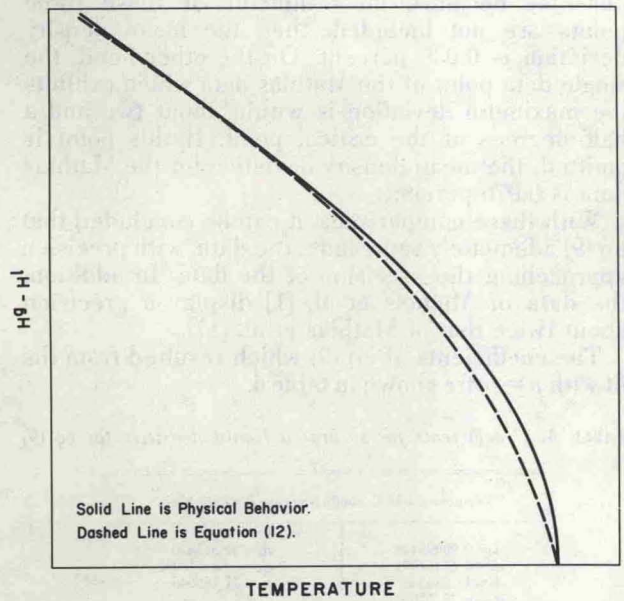

FIGURE 2. *Latent heat of vaporization as a function of temperature.*

Therefore, for this work on argon, the following two approximations were proposed:

$$H^g - H^l = K_1 + K_2 T + K_3 T^2 \qquad (12)$$

and

$$V^g - V^l = \left(1 - \frac{P}{P_c}\right)\frac{RT}{P}. \qquad (13)$$

The approximations suggested by eqs (12) and (13) are compared with the assumptions of eq (11) and are shown in figures 2 and 3.

Figure 2 illustrates a typical plot of the latent heat of vaporization as a function of temperature. It is observed that the third assumption of eq (11), which approximates the latent heat as a constant, is unsatisfactory both in magnitude and in characteristic nature. It is thus proposed that eq (12) represent the latent heat of vaporization. Equation (12) is shown in figure 2 as the dashed line and is seen to represent more closely the characteristic nature of the physical behavior. The constants in eq (12) may be adjusted to change slightly the nature of the curve. Therefore, it was concluded that the quadratic nature of eq (12) satisfactorily represented the physical behavior in figure 2, and no higher degree temperature terms were considered necessary.

Figure 3 illustrates a typical plot of the volume of vaporization as a function of temperature. It is clear that the perfect gas assumption of eq (11)

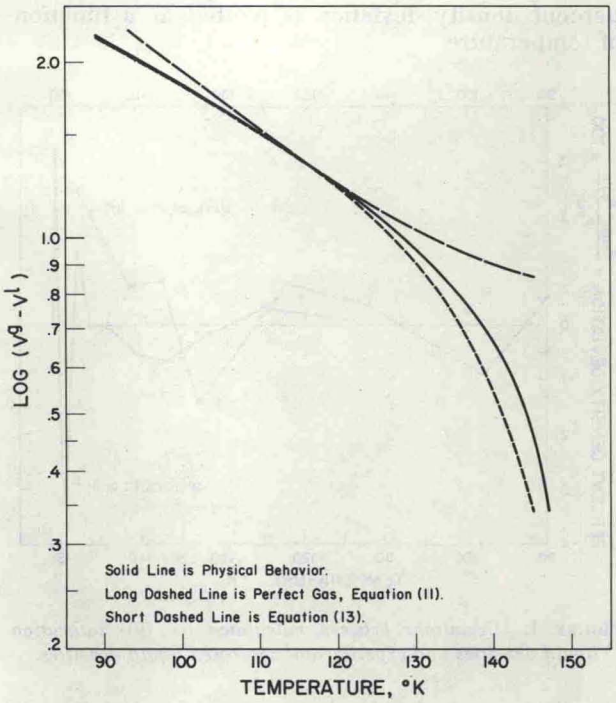

FIGURE 3. *Volume of vaporization as a function of temperature.*

becomes quite unsatisfactory as temperature increases. In addition, it is noted that the characteristic curvature of the perfect gas representation is incorrect. In figure 3, it is seen that the approximation proposed by eq (13) represents the physical behavior more closely and maintains the proper curvature for the entire temperature range. In addition, eq (13) permits the volume of vaporization to reduce to zero as the pressure approaches critical pressure. It should be noted that the deviations between the different models shown in figures 2 and 3 are used only for purposes of illustrating qualitative trends and are not indicative of the actual deviations of the calculated vapor pressure properties.

Substitution of eqs (12) and (13) into eq (10) and integrating give

$$\ln P = A/T + B \ln T + CT + D + EP. \qquad (14)$$

Equation (14) was then the equation which was proposed for representing the vapor pressure data, with five constants to be determined by a least-square fit to the data.

In order to fit the vapor pressure eq (14) to the data, considerations were given to the expermental errors in the observed data points so that each of the data points could be appropriately weighted. The weighting scheme, as described by Hust and McCarty [20], is outlined below.

Let a function with "Q" variables

$$y_n = f(x_{1n}, x_{2n}, \ldots, x_{qn}, \ldots, x_{Qn})$$

$$\text{for } n = 1, 2, \ldots, N \qquad (15)$$

represent the set of "N" experimental data points

$$Y_n, X_{1n}, X_{2n}, \ldots, X_{qn}, \ldots, X_{Qn} \tag{16}$$

where Y_n is the dependent variable for the nth data point and X_{qn} is the qth independent variable for the nth data point. The weighting factor is most usually described as the reciprocal of the variance

$$W=\frac{1}{\sigma_Y^2}, \tag{17}$$

which takes into account the variance of the dependent variable.

Since both the independent and dependent variables affect the final fit of the function to the data, the weight function for the nth data point is expressed as

$$W_n=\frac{1}{\sigma_{Y_n}^2+\sum_{q=1}^{Q}\left(\frac{\partial f}{\partial x_{qn}}\sigma_{qn}\right)^2}. \tag{18}$$

Since P was chosen as the dependent variable in eq (14), Y becomes

$$Y=\ln P-EP. \tag{19}$$

To obtain σ_{Y_n} for eq (18) for the nth data point,

$$\sigma_{Y_n}=\frac{\partial Y}{\partial P_n}\sigma_{P_n}=\left(\frac{1}{P}-E\right)\sigma_{P_n}. \tag{20}$$

Also from eq (18) and the vapor pressure equation (14),

$$\sum_{q=1}^{Q}\left(\frac{\partial f}{\partial X_{qn}}\sigma_{qn}\right)^2=\left(\frac{\partial f}{\partial T_n}\sigma_{T_n}\right)^2 \tag{21}$$

and

$$\frac{\partial f}{\partial T_n}=\frac{B}{T_n}+C-\frac{A}{T_n^2}. \tag{22}$$

If the experimental uncertainty of the nth data point for the qth variable, "ΔX_{qn}", corresponds to a 95 percent confidence interval on the observed X_{qn}, then the standard deviation "σ_{qn}" is related to ΔX_{qn} as

$$\sigma_{qn}=\tfrac{1}{2}\Delta X_{qn}. \tag{23}$$

The vapor pressure equation (14) is a function of pressure and temperature. Applying eq (23), gives

$$2\sigma_{T_n}=\Delta T_n \tag{24}$$

and

$$2\sigma_{P_n}=\Delta P_n. \tag{25}$$

Substituting the necessary expressions into (18), a weighting function for the nth data point is obtained:

$$W_n=\frac{4}{\left(\frac{B}{T_n}+C-\frac{A}{T_n^2}\right)^2\Delta T_n^2+\left(\frac{1}{P_n}-E\right)^2\Delta P_n^2}. \tag{26}$$

Equation (26) was then used as the weighting function for all of the vapor pressure data except the data of Clark et al. [14]. The vapor pressure data of Clark consisted of several hundred observations. The method which Clark used was a comparison of the vapor pressure of argon with that of oxygen as determined by Hoge [21], and using the latter as a measure of the temperature. In this manner, the temperatures were measured with a mercury-in-glass manometer over most of the temperature range. At higher pressures, the temperature was measured with a copper-constantan thermocouple. Clark stated that the measurements were taken with a reproducibility of about 0.05 percent at low pressures. At higher pressures he found that the temperature control on his apparatus would not maintain the temperature constant with the same precision as at the lower temperatures, resulting in an uncertainty of about 0.2 percent in pressure for a given temperature.

Clark et al. [14] published a plot of deviation (from a fitted equation) in $\Delta \log P$ versus $\log P$. From this plot it appeared that there were about three to four times as many data points at low pressures than at pressures near the critical point. From the description of the experimental techniques used, the uncertainty limits, and the variable density distribution of Clark's data, an arbitrary modifying function was developed to modify the weighting function eq (26) for Clark's data. This function, as described by Gosman [22], is

$$M=\frac{1}{5-\frac{375}{T}}-0.28. \tag{27}$$

Since Clark's lower temperature range included more data points than the high temperature range, and since the temperature control on Clark's apparatus was less precise at the higher temperatures, the modifying function (27) was made to reflect the lower reliability at the higher temperatures.

Equation (27) was used to modify the variance of the fit, so that the weighting factor for Clark's data resulted in

$$W_c=\frac{1}{(\sigma/M)^2}. \tag{28}$$

Using eq (28), the final weighting expression for Clark's data is

$$W_c=WM^2, \tag{29}$$

where W is the general weighting function eq (26).

The nine vapor pressure data points of van Itterbeek, Verbeke, and Staes [9] were not used in the final determination of the vapor pressure equation. These nine points were omitted from the final

evaluation because, within a year of the vapor pressure observations of van Itterbeek et al. [9], a new set of vapor pressure data was reported by van Itterbeek, de Boelpaep, Verbeke, Theeuwes, and Staes [16] which deviated considerably from the earlier data [9], but appeared to be more consistent with the vapor pressure observations from other sources.

The uncertainties in the vapor pressure data were estimated from the statements of the investigators, the description of the experimental procedures, the deviations between the different sets of data, and the apparent random deviations of each set of data.

The resulting uncertainties for all of the vapor pressure data were estimated to be

$$\frac{\Delta T}{T}=0.00025$$

$$\frac{\Delta P}{P}=0.00025. \tag{30}$$

Substituting eqs (30) into (26) and (29),

$$W=\frac{4\times 10^8}{6.25\left[\left(B+CT-\frac{A}{T}\right)^2+(EP)^2+1\right]} \tag{31}$$

and for Clark's data,

$$W_c=WM^2. \tag{32}$$

For each data point, the weighting functions (31) or (32) were substituted into the normal least-square equations as shown by Hust and McCarty [20].

In addition, it was considered desirable to make the vapor pressure equation (14) pass through the critical pressure and temperature so as to be consistent with the equation of state at the critical point. This required adding a constraining equation to the normal least-square equations so that the coefficients of the vapor pressure equation would satisfy the least-square criteria, as well as simultaneously constrain the vapor pressure equation to pass through the critical point. The generalized normal least-square equations with constraints are shown by Hust and McCarty [20] and Gosman [22].

A preliminary weighted-least-square fit with one constraint indicated that the low temperature data of van Itterbeek et al. [16] exhibited a scatter of about three to four times as great as the higher temperature data. Since low temperature vapor pressure data from other investigators were available, these low temperature data of van Itterbeek et al. [16] were omitted from the final fit.

The resulting fit of the vapor pressure equation (14) to the data is illustrated in figure 4, where the deviation between the temperature predicted by eq (14) and the experimental temperature is plotted as a function of pressure.

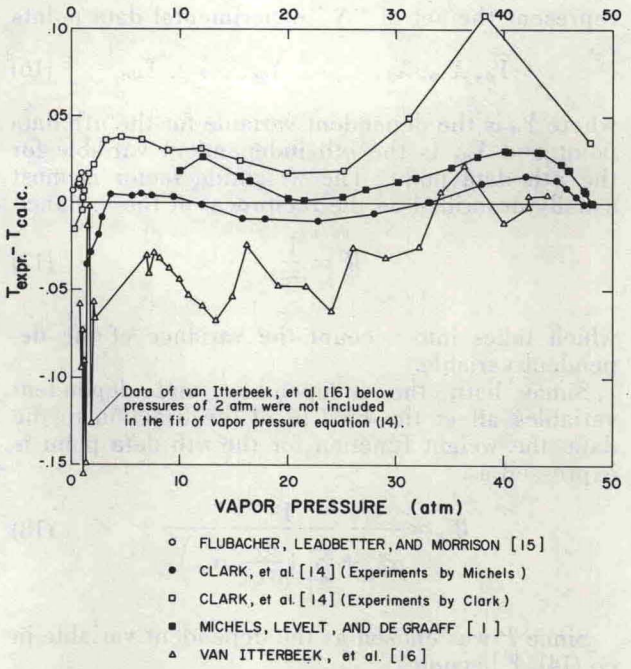

FIGURE 4. *Deviations of vapor pressure data from eq (14).*

In figure 4, it is seen that the characteristic shape of all five of the deviation curves is the same, except for the low temperature data of van Itterbeek et al. [16] (which was not included in the fitted data). From figure 4 it is also noted that the data of van Itterbeek et al. [16] exhibits a pattern of generally wider scatter at the higher temperatures when compared with the other data sources.

The similarity in the basic shape of the deviation curves of figure 4 may be interpreted to indicate a fundamental consistency between the selected vapor pressure data. The deviation curves also indicate the possibility of a disagreement in the temperature scales between the different data sources. This disagreement of temperature scales is inferred from the essentially constant shift or displacement between any one of the deviation curves and any of the others. This displacement of the deviation curves exists despite the fact that an effort was made to convert all of the temperature scales to a common thermodynamic temperature scale. An additional correction of less than 0.01 deg (see sec. 9) was made to the data of Clark et al. [14], since he stated that his data were based on an ice-point temperature of 273.16 K, whereas the other vapor pressure data sources were based on the ice-point temperature of 273.15 K.

From figure 4 it is seen that the maximum temperature deviation is 0.108 deg. This particular point is in the Clark et al. [14] set of data and may be questionable since it contributes a sharp spike in the deviation curve. For Clark's data, the mean of the absolute values of the temperature deviations is 0.0290 deg. If the single questionable data point is omitted, the mean deviation of Clark's data is 0.0240 deg. For the data of Flubacher et al. [15],

the maximum temperature deviation is 0.0174 deg, while the mean of the absolute values of the temperature deviations is 0.0109 deg. The deviations of Clark et al. [14] (experiments by Michels) appear to oscillate slightly about the zero axis except at the lower temperatures where the maximum temperature deviation occurs. For the data of Clark et al. [14], the maximum temperature deviation is 0.0339 deg, while the mean of the absolute values of the temperature deviations is 0.00925 deg. The data of Michels et al. [1] also exhibit a small oscillation with a maximum temperature deviation of 0.0309 deg and a mean of 0.0158 deg. For the data of van Itterbeek et al. [16], the maximum temperature deviation is 0.156 deg, while the mean is 0.0484 deg.

The summary of the deviations between the temperature predicted by the vapor pressure equation (14) and the experimental temperature is given in table 5.

TABLE 5. *Summary of vapor pressure deviations*

Max. temp deviation	Mean abs. temp deviation	Source
0.0339	0.00925	Clark et al. [14].[a]
.108	.0290	Clark et al. [14].
.0309	.0158	Michels et al. [1].
.0174	.0109	Flubacher et al. [15].
.156	.0484	van Itterbeek et al. [16].

[a] Experiments by Michels.

By independent means, Ziegler et al. [2] obtained "best" values for the normal boiling point temperature and triple point temperature. It is important to note the deviations between the temperatures given by Ziegler et al. [2] and the temperatures predicted by the vapor pressure equation (14). The normal boiling point temperature given by Ziegler is 87.280 $\pm$0.015 K, while the normal boiling point temperature predicted by equation (14) is 87.2838 K. The triple point temperature recommended by Ziegler is 83.80 K, while the triple point temperature predicted by eq (14) is 83.8038 K, which corresponds to a temperature deviation of 0.0045 percent.

TABLE 6. *Least squares estimates of coefficients for vapor pressure eq (14)* [a]

Coefficient	Least squares estimate	Standard deviation of coefficient	Significance level [b]
A	-1.062454904×10^{3}	4.993×10^{1}	99.5%+
B	$-4.2714406\,91$	1.056	99.5%+
C	1.524254979×10^{-2}	5.670×10^{-3}	99 %
D	2.992927939×10^{1}	4.796	99.5%+
E	2.465760638×10^{-3}	5.049×10^{-4}	99.5%+

[a] Where P is in atm and T is in K.
[b] These parameters are significant at the level indicated when applying the standard F test.

Table 6 lists the five coefficients for eq (14). Also tabulated in table 6 are the standard deviations and a significance level of these parameters. The significance level indicates these parameters are significant at least to the level indicated when applying the standard F test.

7. The *P-V-T* Surface

Many equations of state have been proposed to represent the *P-V-T* surface. Some of these equations represent the experimental data adequately in limited regions of the thermodynamic surface but are quite inadequate in other regions. Other equations, taking the form of polynomials along isotherms or isochores, are well suited to represent a single source of highly precise experimental data. However, the use of these polynomial expressions becomes very difficult in a complete correlation of the *P-V-T* surface with multiple sets of experimental data with odd spacings of temperature and density.

In this analysis the *P-V-T* surface was basically represented by an equation of state proposed by Benedict, Webb, and Rubin [23] with modifications by Bloomer and Rao [24] and further modified and extended by Strobridge [25].

The Benedict-Webb-Rubin equation was developed by defining and utilizing a quantity $\bar{A}$, called the residual work content. The residual work content was defined as the difference between the Helmholtz function for a real substance and the Helmholtz function for an ideal gas.

The Helmholtz function

$$A=U-TS \tag{33}$$

may be combined with the first and second laws of thermodynamics,

$$dU=TdS-PdV. \tag{34}$$

The resulting relationship is

$$dA=-PdV-SdT. \tag{35}$$

From eq (35),

$$\left(\frac{\partial\bar{A}}{\partial\rho}\right)_T\rho^2=\bar{P} \tag{36}$$

where $\bar{P}$ is the difference in pressure between the real and ideal gas. Then

$$P=\rho RT+\rho^2\left(\frac{\partial\bar{A}}{\partial\rho}\right)_T \tag{37}$$

where the first term on the right side of eq (37) is the ideal gas pressure and the second term is the difference between the real and ideal gas pressure. Benedict et al. [23] proposed an expression for the residual work content which was actually an extension of the Beattie and Bridgeman equation. The extension to the Beattie-Bridgeman equation was

necessary in order to represent more accurately the real fluid properties at densities which were higher than the Beattie-Bridgeman equation could adequately represent. Beattie noted that isometrics could be expressed by an equation of the form

$$(P-\rho RT)/\rho^2=RTF_1(\rho)-F_2(\rho)-F_3(\rho)/T^2. \quad (38)$$

Equations for the functions F_1, F_2, and F_3 were then empirically developed to fit experimental data and, at the same time, remain consistent with the residual work content. By these means, Benedict et al. developed an eight adjustable parameter equation of state for hydrocarbons.

After further modifications, Strobridge [25] extended the Benedict-Webb-Rubin equation to represent more accurately the properties of nitrogen. The Strobridge modifications resulted in an equation with sixteen adjustable parameters.

The form of the equation expressed by Strobridge was the one adopted for the determination of the argon *P-V-T* surface. This form of equation appeared justified because corresponding states theory indicated that there should be reasonable correspondence between nitrogen and argon [18]. The equation of state then used is

$$\begin{aligned} P=\rho RT&+\rho^2(n_1T+n_2+n_3/T+n_4/T^2+n_5/T^4)\\ &+\rho^3(n_6T+n_7)+\rho^4n_8T\\ &+\rho^3(n_9/T^2+n_{10}/T^3+n_{11}/T^4)\exp(-n_{16}\rho^2)\\ &+\rho^5(n_{12}/T^2+n_{13}/T^3+n_{14}/T^4)\exp(-n_{16}\rho^2)\\ &+\rho^6n_{15}. \end{aligned} \quad (39)$$

As a matter of convenience, eq (39) was solved for $Z-1$, and the resulting expression was then fitted to the data by least squares. This expression is

$$\begin{aligned} Z-1=&\frac{\rho}{R}(n_1+n_2/T+n_3/T^2+n_4/T^3+n_5/T^5)\\ &+\frac{\rho^2}{R}(n_6+n_7/T)+\frac{\rho^3}{R}n_8\\ &+\frac{\rho^2}{R}(n_9/T^3+n_{10}/T^4+n_{11}/T^5)\exp(-n_{16}\rho^2)\\ &+\frac{\rho^4}{R}(n_{12}/T^3+n_{13}/T^4+n_{14}/T^5)\exp(-n_{16}\rho^2)\\ &+\frac{\rho^5}{R}n_{15}/T. \end{aligned} \quad (40)$$

A preliminary least squares fit of eq (40) to the selected *P-V-T* data indicated possible round-off discrepancies due to the very large number of arithmetic operations involved with the solution of the normal equations. Therefore, the computer program for the least squares fitting routine was written for double precision arithmetic which carried 20 decimal figures throughout the calculations. This procedure essentially doubled the number of significant figures carried by the computer, so that round-off error due to the large number of arithmetic operations would be minimized.

In addition, an effort was made to check the results of the least squares solution to see if round-off error, due to operating on an ill-conditioned matrix, was present. The method used to perform this check is outlined as follows: The set of normal equations was obtained by standard techniques. The second normal equation in the set was multiplied by a constant and added to the first normal equation. This sum then replaced the original second normal equation. The third normal equation was then multiplied by a different constant and added to the new second normal equation, and so forth. Each of the constant multipliers was, in general, different. The constants were selected so that each of the diagonal elements of the matrix formed by the resulting set of normal equations was larger than the elements to its right. This criterion was used since appreciable loss of accuracy may occur if a diagonal is smaller than elements to its right. The entire check procedure is then equivalent to the rotation of each of the normal equations relative to the others. The solution to the matrix with rotated vectors could then be obtained. If the solution was the same as that for the original matrix, then it was considered likely that a sufficient number of significant figures was carried in the double precision computer solution to make round-off errors insignificant. For the preliminary least squares fit mentioned above, the solution to the matrix with rotated vectors was the same as the original matrix, to eight significant figures. Although eight significant figures is not indicative of the precision of the original *P-V-T* data, the agreement of the two solutions indicated that numerical round-off errors were probably insignificant.

The preliminary least squares fit showed that the data of Walker [11] deviated substantially from those of Michels et al. [1] and Rogovaya et al. [7]. Therefore, the data of Walker were not used in the subsequent fits to eq (40). (Further mention of Walker's data will be made later.)

In the subsequent fits it was found desirable to satisfy the standard least squares criteria and, in addition, to simultaneously constrain eq (40) to exactly satisfy three specific requirements at the critical point. The specific constraints which were used are:

1. The critical isotherm of the equation of state (40) has zero slope at the critical point.

$$\left(\frac{\partial P}{\partial \rho}\right)_T=0 \qquad \text{(critical point)}$$

2. The critical isotherm of the equation of state (40) has a point of inflection at the critical point.

$$\left(\frac{\partial^2 P}{\partial \rho^2}\right)_T=0 \qquad \text{(critical point)}$$

3. The equation of state (40) predicts the critical pressure when the critical density and temperature are substituted into it.

In addition, provisions were made to account for the different uncertainties in the experimental data from the different data sources. The weighting function described by eqs (18) and (23) was used in conjunction with the equation of state (40), where

$$Y=Z-1=\frac{P}{\rho RT}-1 \tag{41}$$

$$\sigma_Y^2=\left(\frac{\Delta Y}{2}\right)^2=\frac{Z^2}{4}\left(\frac{\Delta P}{P}+\frac{\Delta\rho}{\rho}+\frac{\Delta T}{T}\right)^2 \tag{42}$$

$$\left(\frac{\partial f}{\partial x_1}\right)=\left(\frac{\partial(Z-1)}{\partial T}\right)_\rho=\left(\frac{\partial Z}{\partial T}\right)_\rho \tag{43}$$

$$\left(\frac{\partial f}{\partial x_2}\right)=\left(\frac{\partial(Z-1)}{\partial \rho}\right)_T=\left(\frac{\partial Z}{\partial \rho}\right)_T \tag{44}$$

$$2\sigma_T=\Delta T;\ 2\sigma_\rho=\Delta_\rho. \tag{45}$$

Substituting eqs (42) through (45) into eq (18), and simplifying,

$$W=\frac{4}{Z^2\left[\frac{\Delta P}{P}+\frac{\Delta\rho}{\rho}+\frac{\Delta T}{T}\right]^2+\left[T\left(\frac{\partial Z}{\partial T}\right)_\rho\frac{\Delta T}{T}\right]^2+\left[\rho\left(\frac{\partial Z}{\partial \rho}\right)_T\frac{\Delta\rho}{\rho}\right]^2}. \tag{46}$$

The uncertainties in the P-V-T data were estimated from the statements of the investigators, from a knowledge of the experimental apparatus, and from preliminary examinations of the data. The estimated uncertainties associated with the various data are given in table 7.

The uncertainties from table 7 were substituted into eq (46) and weights were calculated for each P-V-T data point. These weights were then substituted into the generalized normal least squares equations with constraints as shown by Hust and McCarty [20].

TABLE 7. *Estimated uncertainties of the experimental data*

% Density	% Pressure	% Temperature	Source
0.05	0.02	0.02	[1]
.05	.02	.02	[6]
.1	.1	.1	[7]
.2	.02	.02	[8]
.2	.02	.02	[9]
.2	.2	.2	[10]

Since the normal equations are linear in the coefficients, the coefficient n_{16} in eq (40) had to be determined before the remaining 15 coefficients were evaluated. A systematic search for the optimum value of n_{16} was performed on the digital computer so that a minimum in the sum of the squares of the deviations was obtained. In order to have a realistic range in the search for n_{16}, an approximate value was obtained by corresponding states with nitrogen. A modified corresponding states method, proposed by Kamerlingh Onnes, was used. This method suggests that the reduced density is

$$\rho_r=\frac{\rho RT_c}{P_c}. \tag{47}$$

The difference between eq (47) and eq (1) is discussed by Gosman [22]. In eq (40), n_{16} appears as the coefficient of a squared density term. From eq (47), a corresponding states expression for a squared density term was obtained:

$$\rho_N^2=\left(\frac{P_c}{T_c}\right)_N^2\left(\frac{T_c}{P_c}\right)_A^2\rho_A^2, \tag{48}$$

where the subscripts N and A represent nitrogen and argon, respectively. Equation (48) was substituted into the exponential term in eq (40). From Strobridge, the n_{16} for nitrogen was also substituted into the exponential term of eq (40). The resulting approximate value of the coefficient n_{16} for argon from corresponding states was calculated to be 0.0039. The range of the systematic search for n_{16} was thus determined to be 0.0039 ± 0.0015. The systematic search was accomplished by incrementing 0.0039 by small values and performing a linear least squares fit for each consecutive value of n_{16}. As the search proceeded, it was found that the sum of the squares of the deviations were not much affected by the current value of n_{16}. However, the fit of the equation of state in the region of the critical point was moderately affected by the different trial values of n_{16}. The resulting value of n_{16} and the least square estimates of the remaining 15 coefficients for eq (40) are given in table 8.

TABLE 8. *Least squares estimates of coefficients for equation of state (40)*[a]

Coefficient	Least squares estimate	Standard deviation of coefficient	Significance level %[b]
n_1	0.25978374×10^{-2}	4.927×10^{-5}	99.5+
n_2	$-.89735867$	3.002×10^{-2}	99.5+
n_3	$-.67273638\times10^{2}$	2.939×10	99.5+
n_4	$-.26494177\times10^{4}$	2.475×10^{2}	99.5+
n_5	$.97631231\times10^{7}$	7.133×10^{5}	99.5+
n_6	$.70478556\times10^{-4}$	1.814×10^{-6}	99.5+
n_7	$-.46767764\times10^{-2}$	1.323×10^{-4}	99.5+
n_8	$.22640765\times10^{-5}$	6.177×10^{-8}	99.5+
n_9	$.48141071\times10^{3}$	8.442×10	99.5+
n_{10}	$.64565346\times10^{5}$	3.152×10^{4}	95.0
n_{11}	$-.11485282\times10^{8}$	2.495×10^{6}	99.5+
n_{12}	$-.64835488$	1.942×10^{-1}	99.5+
n_{13}	$.46524812\times10^{3}$	7.373×10^{2}	25.0
n_{14}	$.10933578\times10^{5}$	1.287×10^{3}	99.5+
n_{15}	$.69439530\times10^{-6}$	4.064×10^{-9}	99.5+
n_{16}	$.48\times10^{-2}$	.....	.....

[a] Where P is in atm, T is in degrees K, ρ is in g-mol/l, and $R=0.0820535$ atm l/g-mol K.

[b] These parameters are significant at the level indicated when applying the standard F test.

316-977 O - 69 - 2

8. Analysis of *P-V-T* Data

Using the coefficients shown in table 8, the equation of state (40) was used to calculate the densities which corresponded to each of the experimental *P-V-T* data points. Percent density deviations between the points calculated by the equation of state and the individual experimental data points which were used in the fit are illustrated in figures 5 through 15. These deviation plots permit the identification of the maximum deviations corresponding to each region of the *P-V-T* surface as well as the specific deviations from each data source.

The deviation plots for the data of Michels et al. [1] and Michels et al. [6] are shown by figures 5 through 11. Inspection of figures 5 and 6 shows that the largest density deviations occur in the vicinity of the 153.15 K isotherm. For this isotherm, the largest deviations occur in the region of the critical point. The same phenomenon occurs for the 163.15 K and 150.65 K isotherms and, to a lesser extent, for the 173.15 K and 148.15 K isotherms. This behavior is illustrated in figures 7 and 8.

Figure 16 illustrates the characteristics of the different isotherms as they range over the pressure-density coordinate system. It is seen that the high and low temperature isotherms have relatively large

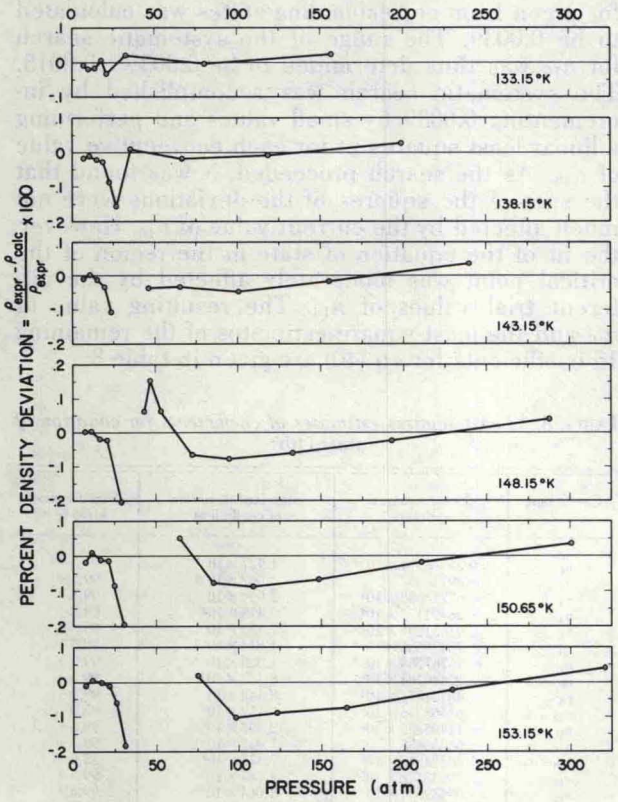

FIGURE 5. *Low temperature density deviations of data by Michels et al. [1] from the equation of state (40).*

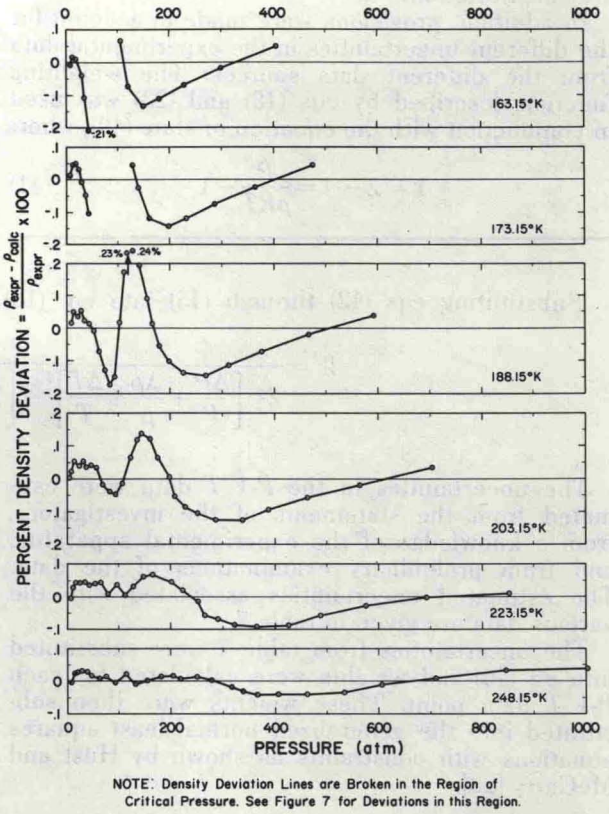

FIGURE 6. *High temperature density deviations of data by Michels et al. [1] from the equation of state (40).*

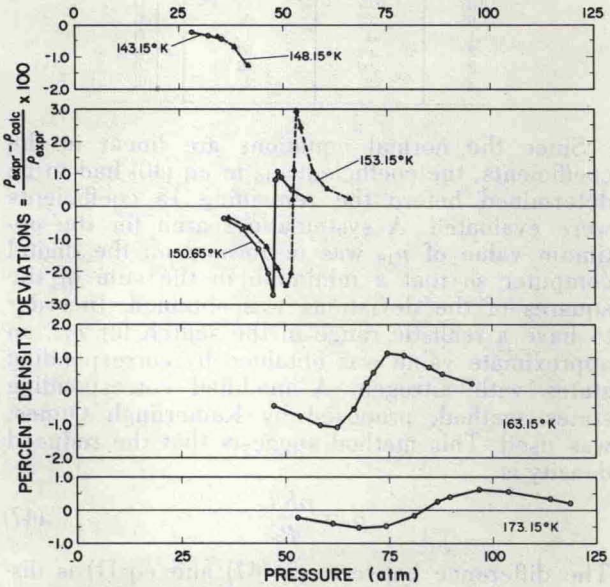

FIGURE 7. *Density deviations in the region of the critical point.*

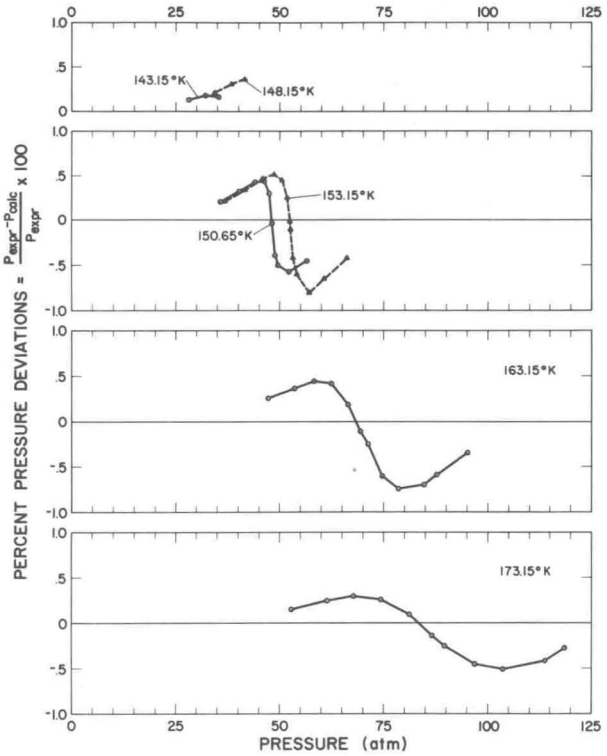

NOTE: These Pressure Deviations are in the Region of the Critical Point as Shown in Figures 5 and 6.

FIGURE 8. *Pressure deviations in the region of the critical point.*

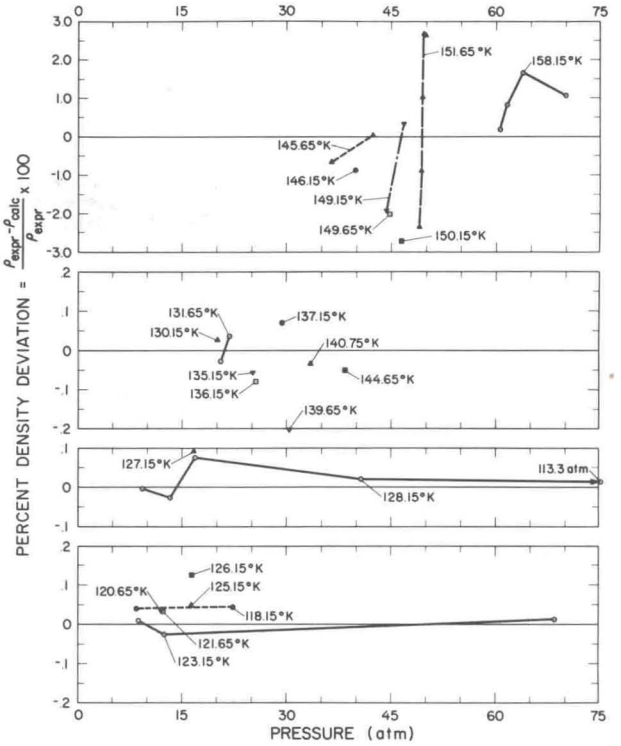

FIGURE 10. *Density deviations for data points near the saturation boundary.*

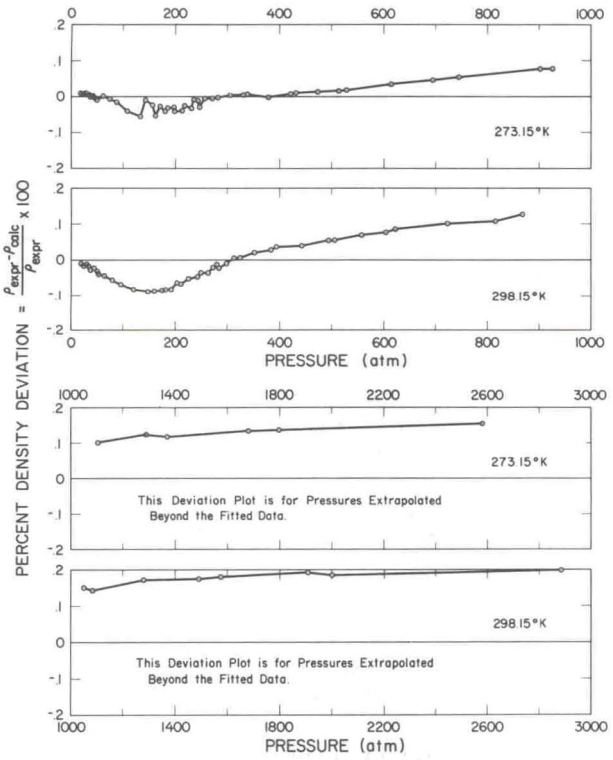

FIGURE 9. *Density deviations of data by Michels et al. [6] from equation of state (40).*

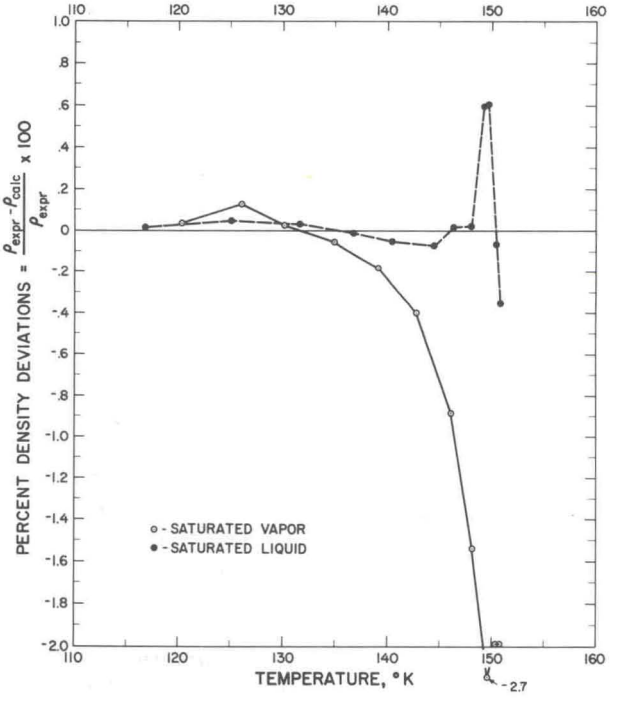

FIGURE 11. *Density deviations of saturation data from equation of state (40).*

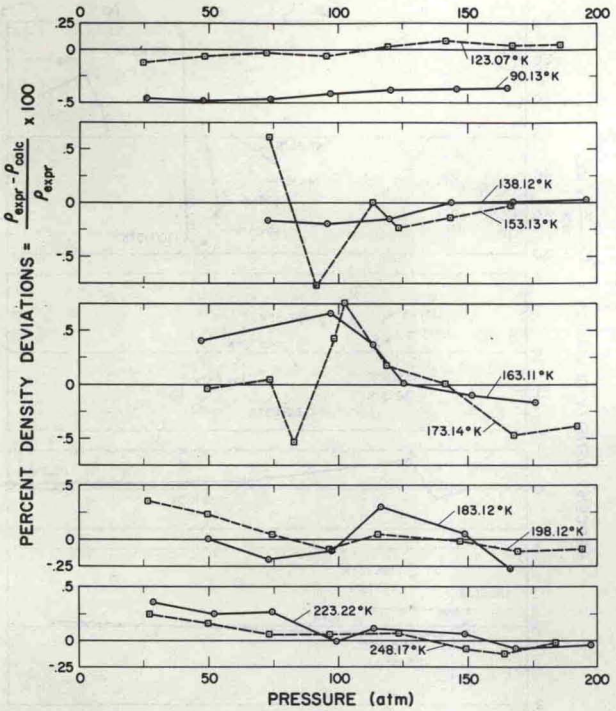

FIGURE 12. *Density deviations of data by Rogovaya et al. [7] from equation of state (40).*

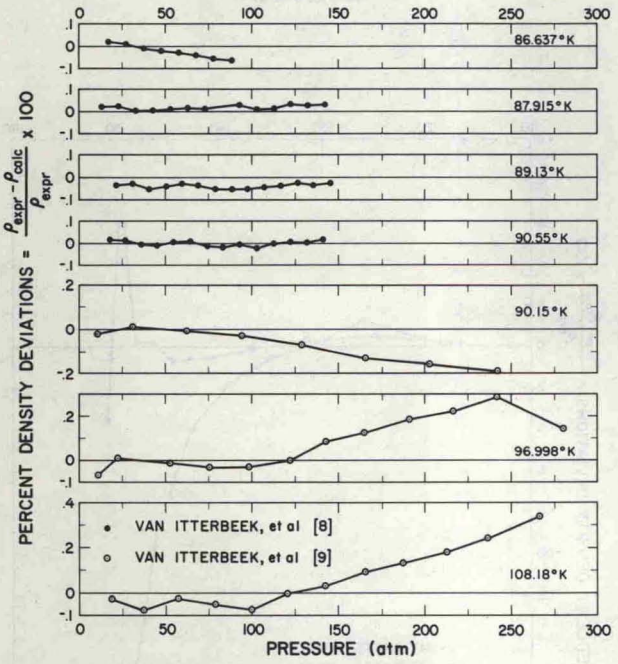

FIGURE 13. *Density deviations of data by van Itterbeek et al. [8, 9] from equation of state (40).*

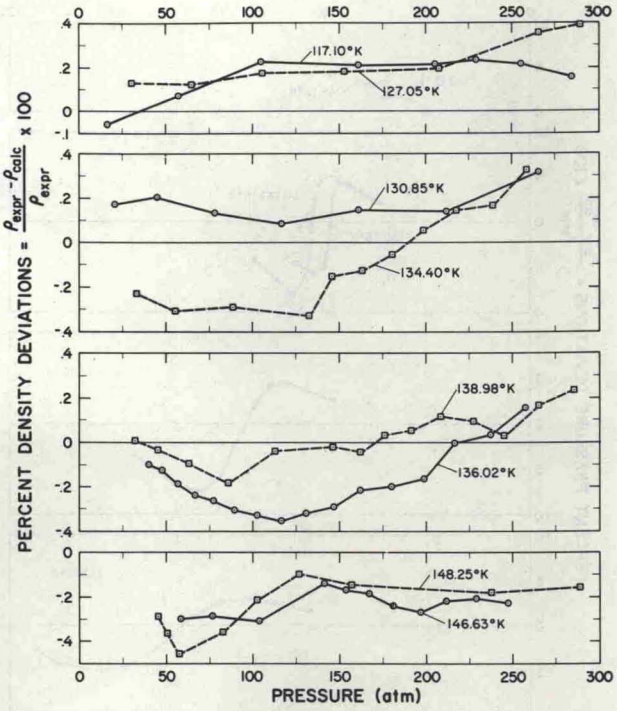

FIGURE 14. *Density deviations of data by van Itterbeek et al. [9] from equation of state (40).*

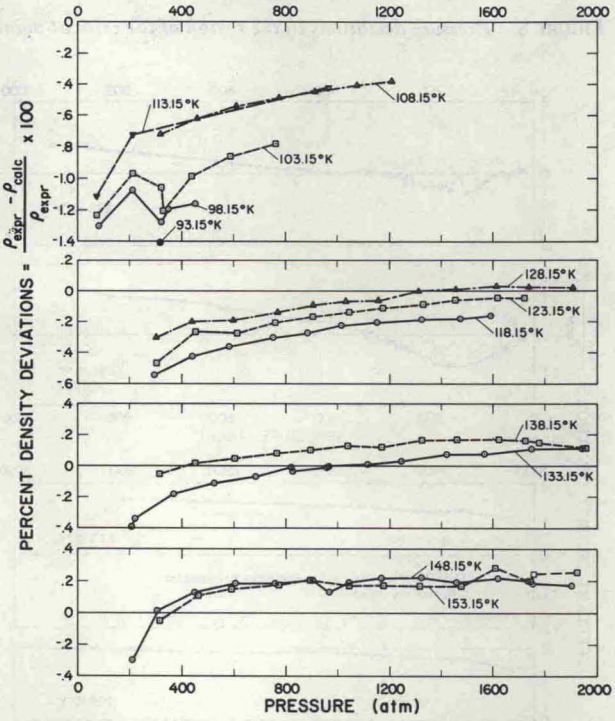

FIGURE 15. *Density deviations of data by van Witzenburg [10] from equation of state (40).*

slopes with not much change in curvature. However, the isotherms between 148 K and 173 K have large variations in the slopes and curvatures. In addition, the slopes of the isotherms in the vicinity of the critical point are small, thus producing large density deviations for rather small pressure or temperature deviations. The small cross-hatched area in figure 16 indicates the region where the density has the great-

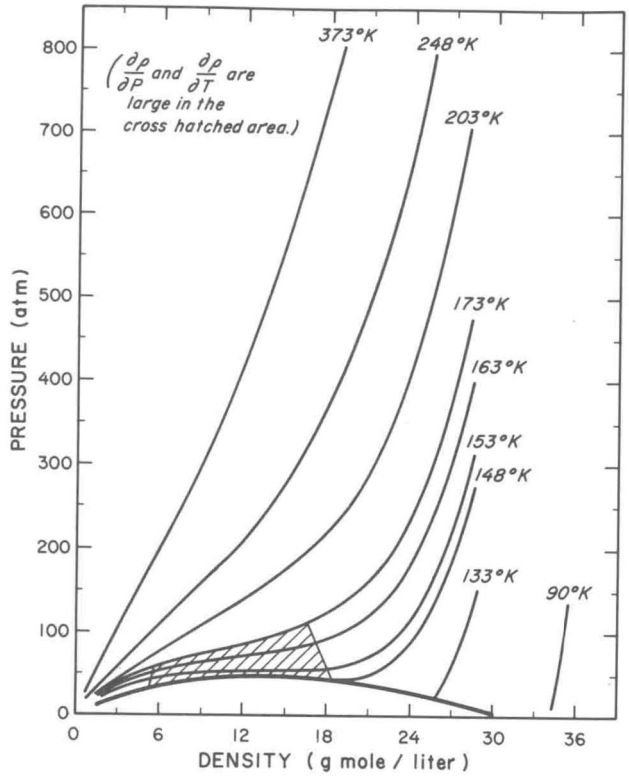

FIGURE 16. *Pressure-density diagram showing isothermal characteristics.*

est sensitivity to small variations in pressure or temperature. If the data points in this region are not included, the mean of the absolute values of the density deviations is 0.08 percent for the data of Michels et al. [1]. If the data points in this region are included, the mean deviation in density becomes 0.26 percent for the data of Michels.

Figures 7 and 8 are expanded-scale deviation plots from figures 5 and 6 and correspond to the region near the critical point. Figure 7 is a density deviation plot and shows a systematic trend which can be attributed to the equation of state. The magnitudes of the density deviations in figure 7 are due to the extreme sensitivity of the density in this region. Figure 8 is a pressure deviation plot for the same region. The systematic trend is still present, but the magnitudes of the pressure deviations are significantly smaller than the corresponding density deviations.

Figure 9 illustrates the density deviations for two isotherms from the data of Michels et al. [6]. A total of 94 data points for these two isotherms were fitted to pressures of about 1000 atm. The mean of the absolute values of the density deviations is 0.034 percent for pressures to 1000 atm, and the data appear to be consistent with the data of Michels et al. [1]. In addition, figure 9 shows density deviation plots for the same two isotherms for pressures from 1000 to about 3000 atm. The equation of state was not fitted to any data above 1000 atm, so the latter deviation plots represent an extrapolation of the equation of state for pressures beyond the fitted data. The density deviations are approximately constant for this pressure range with a mean density deviation of 0.15 percent.

Figure 10 exhibits the density deviations for 41 experimental data points of Michels et al. [1] which are close to the saturation boundary. With the exception of the points close to the critical point the mean density deviation is 0.05 percent. The density deviations for the data close to the critical point are again due to the extreme sensitivity of the density in this region.

Figure 11 is a deviation plot for the saturation line, showing the density deviations between the 23 data points of Michels et al. [1] and the saturation densities calculated by the equation of state. Both saturated liquid and saturated vapor data points are illustrated. With the exception of the saturated liquid data points within about 1.5 K of the critical point, the mean density deviation for the saturated liquid data is 0.03 percent. With the exception of the saturated vapor data points within about 2.5 K of the critical point, the mean density deviation for the saturated vapor data is 0.24 percent.

Figure 12 is the deviation plot for the data of Rogovaya et al. [7]. The mean density deviation is 0.17 percent except for the 90.13 K isotherm. This 90.13 K isotherm appears to be inconsistent with the data of van Itterbeek and Verbeke [8], and van Itterbeek et al. [9], and exhibits a mean density deviation of 0.4 percent. Generally, the data of Rogovaya showed a more random distribution of density deviations than the data from some of the other sources. Rogovaya's data, in general, did not approach the region near the critical point as closely as did Michels et al. [1] and, therefore, no direct comparison of these two data sources is possible in this region where the data are difficult to fit.

Figure 13 illustrates the density deviation plot for the data of van Itterbeek and Verbeke [8]. The mean density deviation for these four isotherms is 0.026 percent. However, the 0.026 percent density deviation of van Itterbeek et al. [8] cannot be directly compared with the deviations of the other data sources since van Itterbeek's data are in the high density–low pressure region of the *P-V-T* surface where the isothermal derivative $(\partial P/\partial \rho)_T$ is large. In this region small displacements in the isotherms result in small density deviations.

Figures 13 and 14 show the deviation plots for the data of van Itterbeek, Verbeke, and Staes [9]. Comparisons of the deviations for isotherms of increasing temperature show a trend of increasing negative density deviations. This trend is not evident in the deviation plots for Michels et al. [1], figures 5 and 6, or Rogovaya et al. [7], figure 12. The mean density deviation is 0.16 percent with the larger deviations occurring at the higher temperatures.

Figure 15 shows the deviation plot for the data of van Witzenburg [10]. The trend here is opposite that of van Itterbeek, Verbeke, and Staes. The data of van Witzenburg exhibit an increasing negative density deviation for increasing temperatures.

However, the van Witzenburg data extend to higher pressures than most of the other data sources for equivalent isotherms, and direct comparisons of density deviations are difficult to make at these higher pressures. The low temperature, low pressure isotherms may be compared with the data of van Itterbeek, Verbeke, and Staes, where it is noted that the van Witzenburg data exhibit density deviations which are about an order of magnitude greater in the negative direction. The mean density deviation for the data of van Witzenburg is 0.30 percent.

Walker [11] displayed his data by isochores. Comparisons with other data sources were difficult to make since most of the other data were obtained isothermally. Therefore, Walker's data were smoothed to a function of the form $P = q_1 + q_2T + q_3T^2$ where the q's are constants. (This function was deemed adequate since the isochoric data of Walker was in the liquid region and exhibited only small deviations from straight lines.) These smoothed isochoric P-T values were plotted and compared with other data sources. This plot showed that the slopes from the fitted function were consistent with the slopes from other data, but the values of the isochores assigned by Walker did not agree with others. This disagreement became greater as the critical point was approached. Therefore, the density values of each of the isochores were redetermined by least squaring the experimental data, one isochore at a time, and extrapolating that isochore to the saturated liquid line. Upon comparison, the original data of Walker deviate from the values predicted by the equation of state by about 2 percent in density, with the deviations increasing to about 10 percent as the critical point is approached. However, when comparing the density deviations between the recalculated least square densities and the densities predicted by the equation of state, the mean deviation was 0.25 percent. This latter comparison is, perhaps, a more valid comparison of Walker's data, since he was not able to actually measure the mass of his sample experimentally. Instead, the density values quoted by Walker were estimated by him from an extrapolation of the isochores to the coexistence line. Private communication from Walker [13] indicated that there were errors in the original values quoted for the densities, especially near the critical point. The new values given to us by Walker [13] agreed much more closely with the values predicted by the equation of state.

Figure 17 illustrates the density deviations for the data of Michels et al. [6]. These data include temperatures above 300 K for pressures to about 2600 atm. Since the equation of state was not fitted to the data in this region, these deviation plots represent an extrapolation of the equation of state for temperatures and pressures beyond the fitted data. The mean density deviation for these data is 0.15 percent for temperatures to 423 K and pressures to 2600 atm, which includes a total of 247 data points. The mean density deviations for

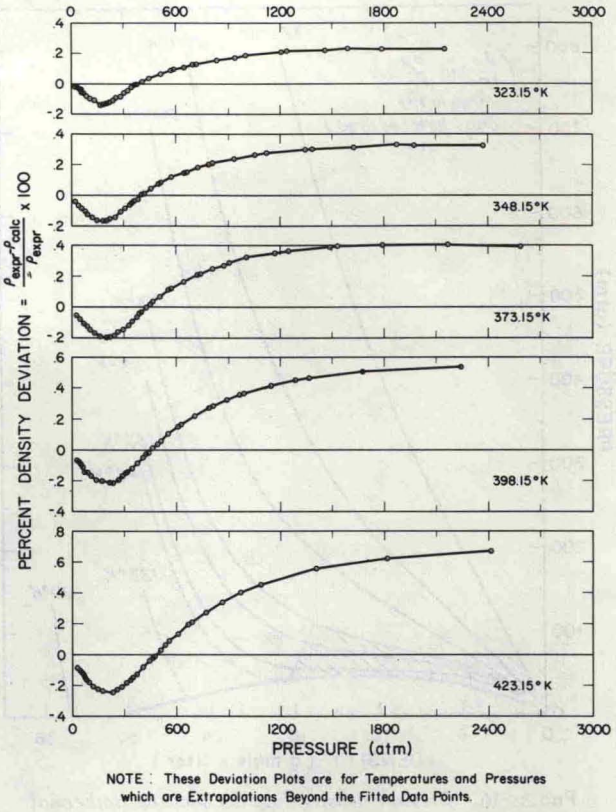

FIGURE 17. *Density deviations for data at temperatures and pressures extrapolated beyond the fitted data points.*

temperatures from 323 to 423 K for pressures to 1000 atm is 0.11 percent. The deviation plots of figures 5 through 17 display varying amounts of systematic deviations between the equation of state and the experimental data. Most of the systematic deviations are small except for the region near the critical point where they become quite marked, as shown in figures 7 and 8. It should be noted that these systematic deviations, although quite small in most cases, are magnified in their contribution to the calculated derivatives.

Although not used for the final fit, the 112 data points of Onnes and Crommelin [26] were compared to the density values predicted by the equation of state. In general, the data of Onnes et al. exhibited a greater scatter than the other data sources, with a mean density deviation of 1.05 percent from the equation of state. Although the Onnes data were limited to pressures below 60 atm, some of the experimental isotherm data overlapped portions of the experimental range investigated by Michels et al. [1]. Generally, the Onnes data showed the same characteristics as the Michels data except for lesser precision. In almost all cases where comparisons could be made, the magnitude of the density quoted by Onnes was smaller than the experimental density of Michels. In a few instances, the Onnes data could be compared with the data of Rogovaya et al. [7]. Again, the densities quoted by Onnes were

smaller than those given by Rogovaya. Some of these latter comparisons indicated that the equation of state predicted density values between those of Onnes and those of Rogovaya.

A final comparison was made between the compilation of the National Bureau of Standards Circular 564 by Hilsenrath et al. [27] and the values predicted by the equation of state. A total of 338 points was used for this comparison. The points were selected so as to well represent the entire range of data compiled by Hilsenrath et al. The temperature range included temperatures from 100 K to 5000 K with pressures ranging from 0.01 to 100 atm. Except for one region, this comparison showed a mean density deviation of 0.08 percent. The one region where the deviations were greatest was at the high pressure–low temperature end of the tables compiled by Hilsenrath et al. (pressures near 100 atm for temperatures near 180 K). For this region, the values of Hilsenrath et al. were obtained essentially by extrapolation of existing experimental data, which may account for the larger deviations.

9. Temperature Scale Conversions

Wherever appropriate, corrections were made to convert the temperatures reported by the investigator to a consistent thermodynamic Kelvin temperature scale based on an ice point of 273.15 K. In some cases the specific temperature scale used by the experimenter was not clearly specified. In these cases, the literature was searched for other papers or information from the same laboratories, and conversions were made from these determinations. Different methods for correcting temperatures are possible, but the following were deemed most appropriate.

Conversions for the data of Michels, Levelt, and de Graaff [1] and Michels, Wijker, and Wijker [6] from the van der Waals Laboratory were made by first correcting the temperatures from the van der Waals thermometer to the International Temperature Scale and then correcting to the thermodynamic temperature scale. The net correction was less than 0.02 °C which is within the precision of the data. The corrections from the van der Waals thermometer to the International Temperature Scale were made by using the information furnished by J. M. H. Levelt-Sengers [28].

The data of Onnes and Crommelin [26], based upon an ice point of 273.09 K, were converted to the International Temperature Scale by

$$T=(t_c+273.09)\,\frac{273.15}{273.09}$$

where t_c is a reported centigrade temperature.

The data of Clark et al. [14], based upon an ice point of 273.16 K, were converted to the International Temperature Scale by

$$T=(t_c+273.16)\,\frac{273.15}{273.16}.$$

Corrections from the International Temperature Scale to the thermodynamic temperature scale were made by using the tabular information furnished by C. R. Barber [29]. The tabular information by Barber is shown in table 9.

TABLE 9. *Conversion from international to thermodynamic temperatures*

Temperature, °C	$T_{th.}-T_{int.}$
−10	0.005
−20	.011
−30	.017
−40	.024
−50	.0295
−60	.034
−70	.0365
−80	.036
−90	.032
−100	.0245
−110	.015
−120	.0025
−130	−.010
−140	−.020
−150	−.024
−183	0

10. Derived Thermodynamic Properties

The calculation of entropy, enthalpy, and internal energy was performed by using the equation of state (40), the zero pressure (ideal gas) and specific heat (c_p°), and the vapor pressure equation (14). The relationships for calculating these derived properties have been described by Gosman [22], and Hust and Gosman [30], and are presented below.

The entropy of the gaseous phase, as well as the saturated vapor, was expressed as

$$S=S_{T_0}^\circ-R\ln\left(\frac{\rho RT}{P_0}\right)+\int_{T_0}^{\rho}\left[\frac{R}{\rho}-\frac{1}{\rho^2}\left(\frac{\partial P}{\partial T}\right)_\rho\right]d\rho+\int_{T_0}^{T}c_p^\circ\,\frac{dT}{T}. \qquad (49)$$

For eq (49) the reference entropy, $S_{T_0}^\circ=3.23367$ J/g−K, for the ideal gas at $P_0=1$ atm, and the normal boiling point temperature at $T_0=87.28$ K was selected from Hilsenrath et al. [27]. The ideal gas specific heat, $c_p^\circ=\frac{5}{2}R=0.520320$ J/g−K, was also taken from Hilsenrath et al.

The enthalpy of the gaseous phase was expressed as

$$H=H_{T_0}^\circ+\int_{T_0}^{\rho}\left[\frac{P}{\rho^2}-\frac{T}{\rho^2}\left(\frac{\partial P}{\partial T}\right)_\rho\right]d\rho+\frac{P}{\rho}-RT+\int_{T_0}^{T}c_p^\circ dT. \qquad (50)$$

Compilations often do not tabulate $H^\circ_{T_0}$. Many times these compilations tabulate $H^\circ_{T_0}-U^\circ_0$, where U°_0 is the ground-state energy. For purposes of consistency with these compilations, a value of $H^\circ_{T_0}-U^\circ_0=45.4119$ J/g (for the ideal gas at 87.28 K) was selected from Hilsenrath [27]. Then, in order to obtain $H^\circ_{T_0}$ for eq (50), a value of $U^\circ_0=192.5197$ J/g was assigned to the ground-state energy. This value of U°_0 was selected so that the enthalpy of the saturated liquid at 1 atm pressure agrees with the value given by Din [31].

The equation of state (40) was then substituted into eqs (49) and (50). Upon integration, the resulting expressions are

$$\begin{aligned}S=S^\circ_{T_0}&-R\ln\left(\frac{\rho RT}{P_0}\right)+\int_{T_0}^{T}\frac{c_p^\circ}{T}\,dT\\&+\rho\left(-n_1+\frac{n_3}{T^2}+\frac{2n_4}{T^3}+\frac{4n_5}{T^5}\right)-\rho^2\left(\frac{n_6}{2}\right)-\rho^3\left(\frac{n_8}{3}\right)\\&-\exp\left(-n_{16}\rho^2\right)\left(\frac{2n_9}{T^3}+\frac{3n_{10}}{T^4}+\frac{4n_{11}}{T^5}\right)/2n_{16}\\&-\exp\left(-n_{16}\rho^2\right)\left(\frac{\rho^2}{2n_{16}}+\frac{1}{2n_{16}^2}\right)\left(\frac{2n_{12}}{T^3}+\frac{3n_{13}}{T^4}+\frac{4n_{14}}{T^5}\right)\\&+\left(\frac{2n_9}{T^3}+\frac{3n_{10}}{T^4}+\frac{4n_{11}}{T^5}\right)/2n_{16}\\&+\left(\frac{2n_{12}}{T^3}+\frac{3n_{13}}{T^4}+\frac{4n_{14}}{T^5}\right)/2n_{16}^2,\end{aligned}\tag{51}$$

and

$$\begin{aligned}H=H^\circ_{T_0}&+\frac{P}{\rho}-RT+\int_{T_0}^{T}c_p^\circ dT+\rho\left(n_2+\frac{2n_3}{T}+\frac{3n_4}{T^2}+\frac{5n_5}{T^4}\right)\\&+\rho^2\left(\frac{n_7}{2}\right)-\frac{1}{2n_{16}}\left(\frac{3n_9}{T^2}+\frac{4n_{10}}{T^3}+\frac{5n_{11}}{T^4}\right)\exp\left(-n_{16}\rho^2\right)\\&-\left(\frac{\rho^2}{2n_{16}}+\frac{1}{2n_{16}^2}\right)\left(\frac{3n_{12}}{T^2}+\frac{4n_{13}}{T^3}+\frac{5n_{14}}{T^4}\right)\exp\left(-n_{16}\rho^2\right)\\&+\rho^5\left(\frac{n_{15}}{5}\right)+\frac{1}{2n_{16}}\left(\frac{3n_9}{T^2}+\frac{4n_{10}}{T^3}+\frac{5n_{11}}{T^4}\right)\\&+\frac{1}{2n_{16}^2}\left(\frac{3n_{12}}{T^2}+\frac{4n_{13}}{T^3}+\frac{5n_{14}}{T^4}\right).\end{aligned}\tag{52}$$

The internal energy was obtained from

$$U=H-P/\rho.\tag{53}$$

The method of calculation proceeded as follows:

a. The properties of the gaseous phase and saturated vapor were calculated with the use of eqs (51), (52), and (53).

b. The volume of vaporization (V^g-V^l) was calculated with the use of the equation of state (40) and the vapor pressure equation (14).

c. The slope of the vapor pressure curve dP/dT was obtained from eq. (14).

d. The entropy and enthalpy changes due to vaporization were calculated with

$$\frac{dP}{dT}=\frac{S^g-S^l}{V^g-V^l}$$

and

$$H^g-H^l=T(S^g-S^l).$$

e. The saturated liquid properties were obtained by subtracting the entropy and enthalpy changes due to vaporization from the saturated vapor value.

f. The saturated liquid line, as calculated in step e, was then used as the datum point for calculating properties below the critical temperature and densities greater than those of the saturated liquid. These properties were calculated by the isothermal integration of the appropriate portions of eqs (49) and (50). These expressions are

$$S = S^l - \int_{\rho^l}^{\rho} \left[\frac{1}{\rho^2} \left(\frac{\partial P}{\partial T} \right)_\rho \right] d\rho$$

and

$$H = H^l + \frac{P}{\rho} - \frac{P}{\rho^l} + \int_{\rho^l}^{\rho} \left[\frac{P}{\rho^2} - \frac{T}{\rho^2} \left(\frac{\partial P}{\partial T} \right)_\rho \right] d\rho.$$

By progressing through the above procedure, the derived properties were calculated for the entire portion of the thermodynamic surface under consideration. However, the method of calculation outlined above may result in a discontinuity. This discontinuity exists at temperatures below the critical temperature for pressures above the critical pressure. The cause of the discontinuity arises from the fact that the calculation of the derived properties was performed by one procedure for temperatures above the critical temperature and a second procedure for temperatures below the critical. For temperatures below the critical, the changes of entropy and enthalpy due to vaporization had to be calculated as outlined in step d, and the saturated liquid line obtained as outlined in step e. For temperatures above the critical, steps d and e were not needed for the calculation of derived properties. The mutual boundary (at the critical temperature) between these two regions then exhibited the discontinuity. This discontinuity in the derived properties is possibly due to slight disagreement between the isochoric slope of the equation of state (40) at the critical point and the slope of the independently obtained vapor pressure equation (14) at the same point.

When the discontinuities were plotted with a highly expanded scale, it was determined that the discontinuity was independent of pressure. Adjustments to the derived properties were then determined by smoothing the transition region for isobars near the critical. These adjustments were applied to the derived properties by making appropriate corrections to the entropy and enthalpy of vaporization. The adjustments were added to the entropy and enthalpy of vaporization, thus decreasing the values for the entropy and enthalpy of the saturated liquid. Table 10 lists the temperature dependent adjustments which were made.

All of the data which have been calculated were restricted to the liquid and gaseous regions by using

TABLE 10. *Adjustments for entropy and enthalpy of the saturated liquid*

Temperature K	Entropy J/g−K adjustment [a]	Enthalpy J/g adjustment [a]
150	0.009539	1.431
149	.009750	1.453
148	.008768	1.298
147	.007549	1.110
146	.006330	0.924
145	.005189	.752
144	.004160	.599
143	.003249	.465
142	.002460	.349
141	.001789	.252
140	.001239	.173
139	.000811	.113
138	.000490	.068
137	.000260	.036
136	.000100	.014
135	.000010	.001

[a] These adjustments have been subtracted from the entropy and enthalpy of the saturated liquid.

the following melting curve relationship:

$$P_{\text{melt}} = P_t + A \left[\left(\frac{T_{\text{melt}}}{T_t} \right)^C - 1 \right]. \tag{54}$$

In eq (54), A and C are constants which were determined by a least squares fit to experimental data. The form of this melting curve relationship is discussed by Goodwin and Weber [32].

The experimental data which were considered for the determination of the constant in eq (54) were taken from Michels and Prins [33], Lahr and Eversole [34], and Bridgman [35]. The constants of eq (54) were determined to be

$$A = 2078.76667$$
$$C = 1.59817868,$$

with a mean of the absolute pressure deviations of 0.08 percent.

The properties, density, enthalpy, internal energy, and entropy, are presented as functions of pressure and temperature in the tables of appendix A. The number of significant figures given in these tables is not justified on the basis of the uncertainties of the data, but, rather, is desirable to maintain the internal consistency of the tables.

A comparison of the heat of vaporization was made at the normal boiling point. The heat of vaporization of various investigators was compared with the value obtained by using the equation of state (40) and vapor pressure equation (14). This comparison is shown in table 11.

TABLE 11. *Comparison of heat of vaporization at the normal boiling point*

Frank and Clusius [36]	1557.5 ± 1.5	cal/g-mol
Flubacher et al. [15]	1555 .0 ± 4.6	cal/g-mol
Eucken [37]	1501	cal/g-mol
Ziegler et al. [2]	1543.4	cal/g-mol
This work	1546.3	cal/g-mol

11. Equation of State and Saturation Boundary

The saturation boundary can be defined by the equation of state if there is a sufficient number of highly precise experimental *P-V-T* data points along the entire boundary. However, saturation densities are difficult to measure with high precision. In addition, for argon there was only one source of satisfactory saturation data, and these data did not cover the entire two-phase boundary. Therefore, it was difficult to perform a critical evaluation of these saturation data for the purpose of determining the saturation boundary.

Instead, there was available a relatively large number of *P-T* data points along the saturation boundary. For these data, the vapor pressure equation (14) was developed. Therefore, the definition of the saturation boundary was obtained by the use of two independent equations—the equation of state (40) and the vapor pressure equation (14).

The saturation boundary, as defined by the equation of state alone, was then examined for internal thermodynamic consistency by using the conditions of thermodynamic equilibrium:

$$\begin{aligned} T^l &= T^g \\ P^l &= P^g \\ G^l &= G^g. \end{aligned} \tag{55}$$

The equation of state (40) is a continuous function with a van der Waals form across the saturation boundary. Therefore, the equation for thermodynamic equilibrium (55) could be substituted into the equation of state (40). This was accomplished for a given saturation temperature by imposing the equilibrium conditions upon both the equation of state and the equation for the Gibbs function derived from the equation of state and solving them iteratively and simultaneously for the corresponding density. By this means the entire saturation boundary was derived by the use of the equation of state and the conditions of thermodynamic equilibrium, without using the independently obtained vapor pressure equation (14).

A comparison of the vapor pressures as derived from the equation of state and the vapor pressures as obtained from the vapor pressure equation was made. The results of this comparison are shown in table 12 for 5-deg temperature increments.

The agreement shown in table 12 indicates that the equation of state is internally consistent with the conditions of thermodynamic equilibrium. Table 12 also indicates that the equation of state satisfactorily predicts *P-V-T* values in the vicinity of the saturation boundary.

TABLE 12. *Vapor pressure comparison*

T, K	P_1, Atm	P_2, Atm	P_1-P_2
85	0.77945	0.79737	−0.01792
90	1.32133	1.34210	−.02077
95	2.11103	2.13029	−.01926
100	3.20974	3.22249	−.01275
105	4.68121	4.68277	−.00156
110	6.59102	6.57784	.01318
115	9.00650	8.97649	.03001
120	11.99740	11.94960	.04780
125	15.63733	15.57082	.06651
130	20.00587	19.91829	.08758
135	25.19168	25.07827	.11341
140	31.29662	31.15296	.14366
145	38.44154	38.28020	.16134
150	46.77419	46.71197	.06222

P_1 is calculated from vapor pressure equation (14).
P_2 is calculated from equation of state (40).

12. Second Virial Coefficient and Intermolecular Potential

An equation of state which has been extensively used is

$$\frac{PV}{RT} = Z = 1 + B\rho + C\rho^2 + D\rho^3 + \ldots, \tag{56}$$

where B, C, D, . . . are virial coefficients and represent deviations from ideal gas behavior. The virial coefficients are functions of temperature and are related to interactions between molecules. The second virial coefficient, B, is related to interactions between two molecules, the third virial, C, to the interaction between three molecules, etc. When the gas has negligible molecular interaction as compared to interaction with the walls of the confining vessel, then eq (56) reduces to the perfect gas where $Z=1$.

The virial coefficients for the equation of state (40) were obtained by arranging the equation of state into virial form as shown in eq (56). In order to obtain the proper form, the exponential term of eq (40) was expanded as

$$\exp(-n_{16}\rho^2) = 1 - (n_{16}\rho^2) + \frac{(n_{16}\rho^2)^2}{2!} - \frac{(n_{16}\rho^2)^3}{3!} + \ldots. \tag{57}$$

Substituting eq (57) into eq (40),

$$\begin{aligned} Z = 1 &+ \rho\left(\frac{n_1}{R} + \frac{n_2}{RT} + \frac{n_3}{RT^2} + \frac{n_4}{RT^3} + \frac{n_5}{RT^5}\right) \\ &+ \rho^2\left(\frac{n_6}{R} + \frac{n_7}{RT} + \frac{n_9}{RT^3} + \frac{n_{10}}{RT^4} + \frac{n_{11}}{RT^5}\right) + \rho^3\left(\frac{n_8}{R}\right) \\ &+ \rho^4\left(\frac{n_{12}}{RT^3} + \frac{n_{13}}{RT^4} + \frac{n_{14}}{RT^5} - \frac{n_{16}n_9}{RT^3} \right. \\ &\left. - \frac{n_{16}n_{10}}{RT^4} - \frac{n_{16}n_{11}}{RT^5}\right) + \ldots. \end{aligned} \tag{58}$$

In eq (58), the coefficient of ρ is the second virial coefficient, the coefficient of ρ^2 is the third virial coefficient, etc.

The second virial coefficient was calculated from eq (58). These coefficients, as functions of temperature are listed in table 13. A comparison between the second virial coefficient calculated by using the virial equation of state (58) and other published data is shown in figure 18.

Except for the data of Kerr [39], figure 18 illustrates that eq (58) represents the second virial coefficients within the uncertainty of the data for temperatures from about 120 to 300 K. Kerr's virial data do not appear to have the precision of the other data sources. For temperatures below 120 K, eq (58) appears to predict virial coefficients which are about 2 percent high. Fender and Halsey [40] estimate their error to be about 1.5 percent, and it is therefore concluded that eq (58) is a satisfactory representation of the virial coefficient data.

TABLE 13. *Second virial coefficients as calculated from virial equation of state (58)*

Temp. K	B	Temp. K	B
90	−215.22	200	−47.18
100	−180.09	210	−42.20
110	−152.39	220	−37.79
120	−130.32	230	−33.86
130	−112.47	240	−30.33
140	− 97.84	250	−27.15
150	− 85.69	260	−24.27
160	− 75.47	270	−21.65
170	− 66.78	280	−19.26
180	− 59.31	290	−17.07
190	− 52.83	300	−15.05

B has units of cm³/mol.

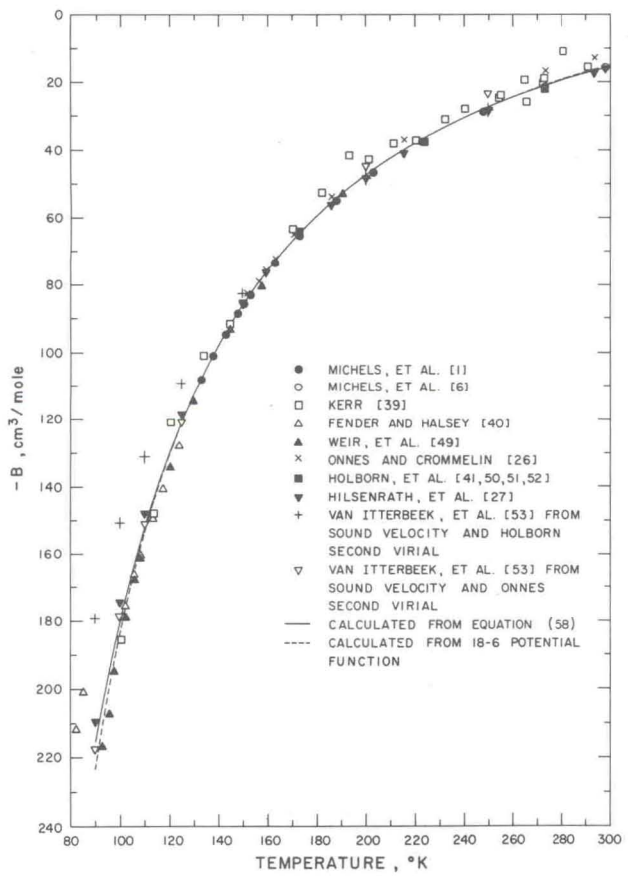

FIGURE 18. *Comparison of second virial coefficients.*

The second virial coefficient may also be theoretically calculated if a mathematical model for the intermolecular force potential is selected. A number of force potentials have been advanced and some of these are discussed in Hirschfelder, Curtiss, and Bird [38] and Gosman [22].

The Lennard-Jones 12–6 model for the potential function is the one most commonly used and was therefore investigated. The expression for the energy for the 12–6 potential is

$$E=4\epsilon\left[\left(\frac{\sigma}{r}\right)^{12}-\left(\frac{\sigma}{r}\right)^{6}\right]. \tag{59}$$

Using eq (59), the expression for the reduced second virial coefficient is obtained as illustrated by Gosman [22]:

$$B^*=\sum_{k=0}^{\infty}\left[-\frac{2^{\left(\frac{2k+1}{2}\right)}}{4k!}\,\Gamma\left(\frac{2k-1}{4}\right)\right]T^{*\left(-\frac{2k+1}{4}\right)}. \tag{60}$$

With eq (60) and the equations

$$T^*=\frac{kT}{\epsilon}$$

$$b_0=\frac{B}{B^*}$$

$$b_0=\frac{2}{3}\pi N\sigma^3, \tag{61}$$

the two parameters ϵ and σ were obtained by the method described in Gosman [22].

It was found that the two parameters, ϵ and σ, of the 12–6 potential are not truly constants, but are somewhat temperature dependent. It was also found that the higher temperature isotherms (about 300 K) are relatively insensitive to variations in the parameters. At the lower temperatures, however, relatively small variations in the parameters result in large variations in the second virial coefficient. This effect was demonstrated for argon by Gosman [22] and shown to be a general property of the relationship between second virial coefficients and potential functions by Hanley and Klein [44].

For the temperature range of 90 to 300 K a set of parameters for the Lennard-Jones 12–6 potential was determined to be

$$\epsilon/k=112.4\text{ K}$$

$$b_0=57.7\text{ cm}^3/\text{mol}.$$

Using these parameters, the mean deviation in B from values calculated by eq (58) was 0.78 cm³/mol.

It is of interest to compare the values of these parameters with values determined by other sources. Holborn and Otto [41] found $\epsilon/k = 122$ and $b_0 = 49.58$ for temperatures between 173 and 673 K. Michels, Wijker, and Wijker [6] found $\epsilon/k = 119.8$ and $b_0 = 49.8$ for temperatures between 273 and 423 K. Since the latter two sets of parameters were obtained for relatively high temperature data, it is expected that the value of ϵ/k would be larger than that obtained in this evaluation.

Since the 12–6 potential appears to be satisfactory for limited temperature ranges only, other forms of the potential function were investigated. Using the basic technique developed by Hanley [42] the family of "m-6" functions was evaluated along with the Kihara potential function. The "m-6" functions were calculated by using the values of the reduced second virial coefficients as presented by Klein [43]. The results of these calculations are shown in figure 19.

Figure 19 shows the deviations between second virials as calculated by the various potential functions and those calculated by the virial eq (58). The deviations in second virial for the 12–6, 15–6, 18–6, and Kihara potential functions are all illustrated in figure 19. It is noted that the Kihara and the 15–6 functions are almost identical over the whole temperature range. This similarity between potential functions is discussed by Hanley and Klein [44]. For the temperature range of 90 to 300 K the set of parameters for the Kihara potential was determined to be

$$\epsilon/k = 125 \text{ K}$$
$$\rho_0 = 3.711 \text{ Å}$$
$$a = 0.080 \text{ Å}.$$

Using these values for the Kihara potential, the mean deviation in B from values calculated by eq (58) was 0.53 cm³/mol.

The 18–6 potential shows a negligibly small deviation in second virial above 120 K. Below 120 K, figure 19 shows that the virials calculated by the 18–6 function deviate from those calculated by eq (58). However, this was the temperature range where eq (58) predicted virials which were 2 percent too large. A comparison of the virials calculated by the 18–6 function with the original data shows that the 18–6 function predicts the virial coefficients to about the uncertainty of the data. The 18–6 function is also shown in figure 19 to illustrate this point.

The parameters for the 18–6 function were determined to be

$$\epsilon/k = 157.5 \text{ K}$$
$$\sigma = 3.28 \text{ Å}.$$

Using these values for the 18–6 function, and omitting the deviations below 120 K, the mean deviation in B is 0.14 cm³/mol.

A final calculation was made for the second virial coefficient to determine the corrections due to quantum effects. The relationships which were used to calculate these second virials with quantal corrections for both the 12–6 and the Kihara potentials are given by Hirschfelder et al. [38]. The results indicated that the quantal corrections are a fraction of one percent, even at the lower temperatures. The magnitude of the quantal correction is within the uncertainty of the published experimental data.

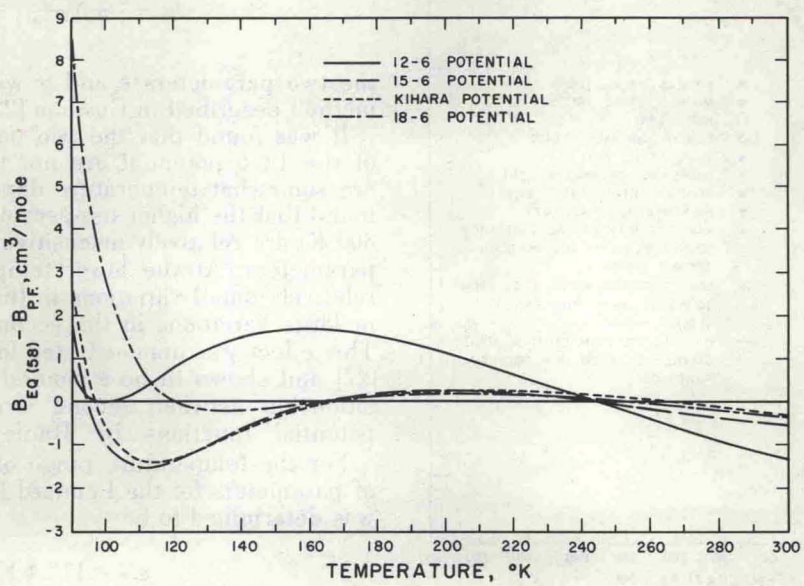

FIGURE 19. *Potential function comparison.*

13. The Joule-Thomson Inversion Curve

The Joule-Thomson coefficient, μ, is defined as the slope of an isenthalpic curve on the P-T coordinate system:

$$\mu=\left(\frac{\partial T}{\partial P}\right)_H. \tag{62}$$

Equation (62) may be rewritten for more convenient evaluation with the equation of state (39):

$$\mu=\frac{1}{C_p}\left[\frac{T}{\rho^2}\frac{\left(\frac{\partial P}{\partial T}\right)_\rho}{\left(\frac{\partial P}{\partial \rho}\right)_T}-\frac{1}{\rho}\right]. \tag{63}$$

The Joule-Thomson inversion curve is defined as the locus of points where $\mu=0$, and may be calculated from

$$\frac{T}{\rho^2}\frac{\left(\frac{\partial P}{\partial T}\right)_\rho}{\left(\frac{\partial P}{\partial \rho}\right)_T}=\frac{1}{\rho}. \tag{64}$$

In eq (64), the partial derivatives were evaluated from the equation of state (39). Equation (64) was programmed for an iterative solution to find the values of density and temperature which satisfied the equation. Pressure values were then calculated from the equation of state for the appropriate densities and temperatures.

The Joule-Thomson inversion curve data as calculated by eqs (64) and (39), are given in table 14 for 10-deg intervals.

TABLE 14. *Inversion curve from eq (64)*

Temp. K	Pressure Atm	Temp. K	Pressure Atm
130	69.27	220	431.68
140	128.64	230	454.08
150	181.92	240	473.88
160	229.83	250	491.23
170	272.96	260	506.28
180	311.83	270	519.19
190	346.81	280	530.07
200	378.27	290	539.04
210	406.48	300	546.22

Figure 20 illustrates the inversion curve and shows the comparison with other data sources. The solid line represents the locus of inversion curve points as calculated by eqs (64) and (39). The solid line is terminated at 300 K, which is the temperature limit of the data fitted by the equation of state (39). The dashed portion of the inversion curve above 300 K represents the locus of points as calculated by eq (64) with data from the equation of state which have been extrapolated beyond the fitted region.

Figure 20 also shows the inversion curve data obtained by Roebuck and Osterberg [45] in 1934. In 1940, Roebuck and Osterberg [46] published a paper indicating that a numerical error in the pressure data had been made. Therefore, the Roebuck and Osterberg [45] data shown in figure 20 have been adjusted by the appropriate correction. The mean of the absolute values of the deviation in inversion temperatures between the corrected data of Roebuck and the values calculated by eq (64) is 1.1 percent.

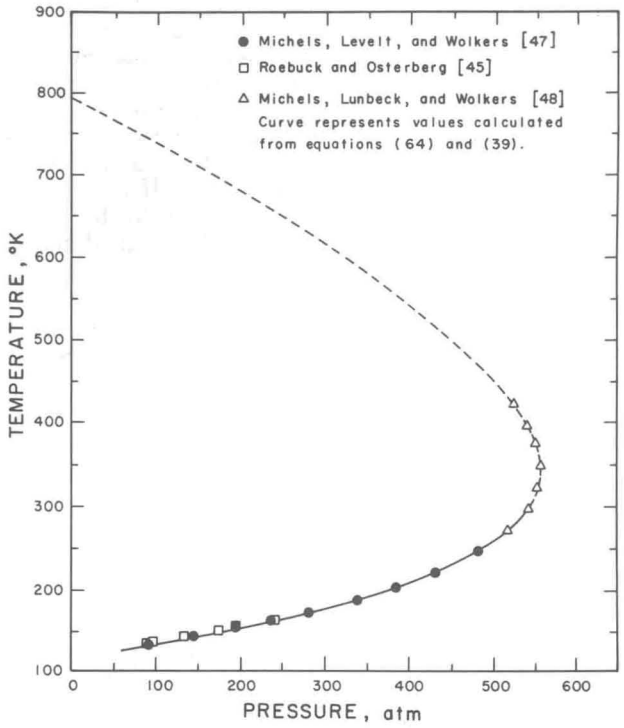

FIGURE 20. *Inversion curve comparisons.*

Michels, Levelt, and Wolkers [47] published Joule-Thomson coefficient data for temperatures from 133 K to 273 K. From these data, the inversion curve pressures and temperatures were obtained by determining where the Joule-Thomson coefficient was equal to zero. The inversion curve data of Michels et al. [47] determined in this manner, are shown in figure 20. The mean deviation between the Michels inversion curve temperatures and the temperatures calculated by eq (64) is 0.30 percent.

Michels, Lunbeck, and Wolkers [48] published Joule-Thomson coefficient data for temperatures from 273 to 423 K. Although the equation of state was not fitted to data above 300 K, a comparison of the data of Michels and the calculated inversion curve is shown in figure 20. The mean deviation in inversion temperatures between the Michels et al. [48] data and the extrapolated values of eq (64) is 1.1 percent.

The maximum inversion temperature as calculated by eq (64) is about 794 K. Based on the Lennard-Jones 12–6 potential, Hirschfelder et al. [38] shows that the theoretical maximum reduced

inversion temperature is 6.47. With this value of reduced temperature and a selected value for the ϵ/k parameter of the 12–6 potential, the theoretical maximum inversion temperature was calculated. If the value, $\epsilon/k=122$, obtained by Holborn and Otto [41] for temperatures up to 673 K is used, the theoretical maximum inversion temperature is 789 K. The deviation between the theoretical maximum inversion temperature and the value calculated by eq (64) is about 0.6 percent. If the value, $\epsilon/k=119.8$, obtained by Michels et al. [6] for temperatures up to 423 K is used, the theoretical maximum inversion temperature is 775 K, giving a deviation of about 2.5 percent. Based upon the 18–6 potential, with a value of $\epsilon/k=157.5$, the theoretical maximum inversion temperature is 770 K, giving a deviation of about 3 percent from the value calculated by eq (64).

The significance of the inversion curve as a test for the equation of state (39) may be seen by noting that the inversion curve eq (64) involves derivatives of the equation of state. As illustrated in figure 20 and as previously mentioned, the deviations between the calculated inversion curve and the data from other sources are relatively small. Therefore it may be concluded that the geometric slope of the physical thermodynamic surface is adequately described by the equation of state (39).

14. Specific Heats

The specific heats of a gas at constant pressure and constant volume are given by

$$C_v=T\left(\frac{\partial S}{\partial T}\right)_v \tag{65}$$

and

$$C_p=T\left(\frac{\partial S}{\partial T}\right)_p. \tag{66}$$

The C_p and C_v illustrated in figures 21 and 22 were calculated by forming the $\left(\frac{\partial S}{\partial T}\right)_v$ and $\left(\frac{\partial S}{\partial T}\right)_p$ numerically with $(\Delta S/\Delta T)_v$ and $(\Delta S/\Delta T)_p$, where ΔT was 0.005 K and ΔS was calculated using the equations given in section 10. These numerically obtained values were compared with values calculated from continuous analytical expressions derived

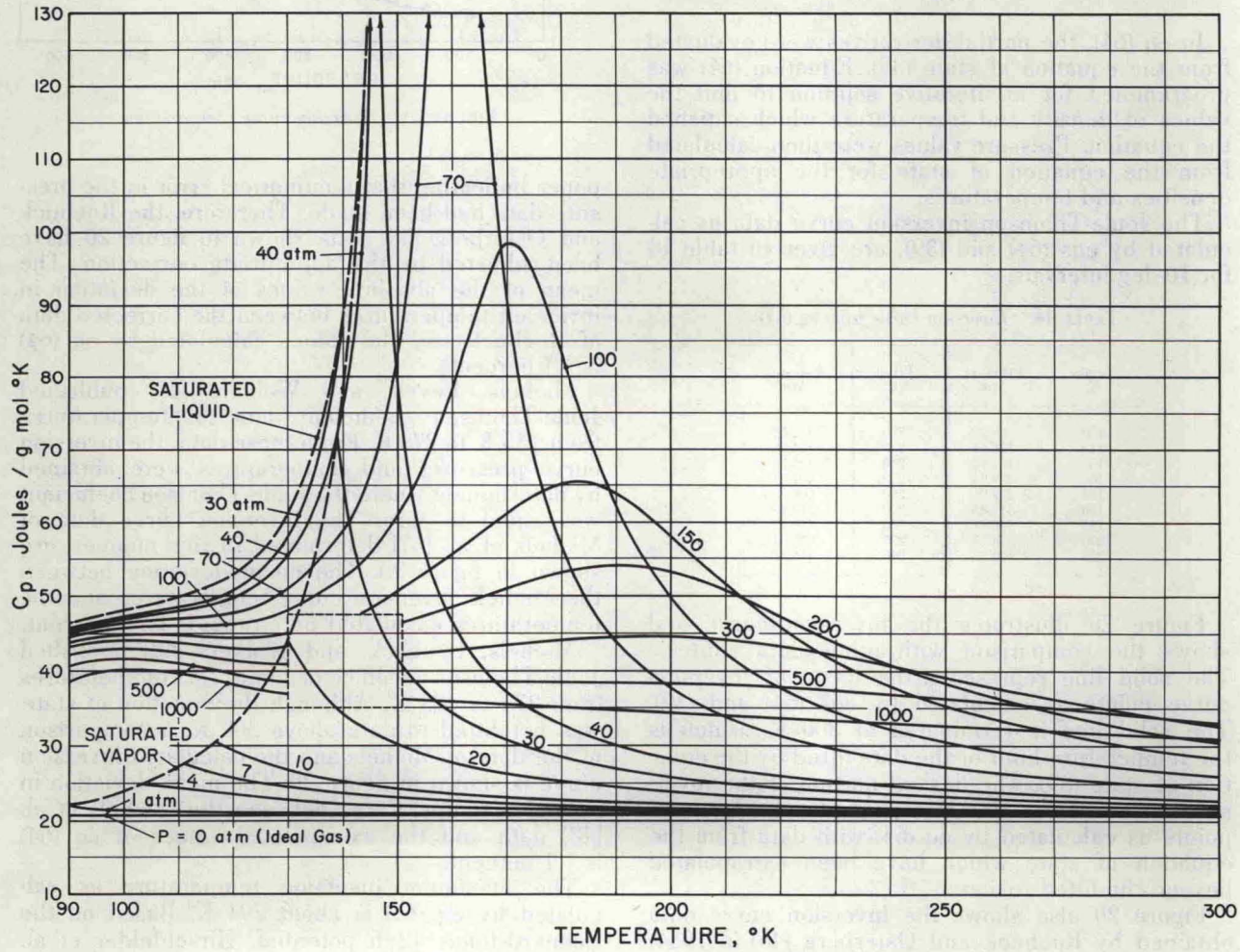

FIGURE 21. *Specific heat at constant pressure calculated by numerical method.*

from the equation of state (39). Such comparisons were made in all regions of the *P-V-T* surface except the compressed liquid region where the continuous expressions were not possible. The differences in the specific heats obtained by the two methods were on the order of 10^{-5} of the total value.

Both the C_v and the C_p diagrams omit the isobars above 100 atm between 130 and 150 K, i.e., areas enclosed by dashed boxes (figs 21, 22). The specific heats calculated from the equation of state in this range of temperature and pressure exhibited erratic behavior inconsistent with the rest of the surface. This behavior is probably caused by the adjustments made to the entropy and enthalpy values for the saturated liquid (see sec. 10).

Comparisons were made between experimental specific heat data and values calculated from the equation of state. With the exception of the low temperature compressed liquid region and the critical region the agreement was good. The deviations were usually less than 5 percent and averaged about 1 percent. Experimental C_v specific heat data near the critical point such as the data of Voronel et al. [54] disagree with the values calculated from the equation of state by as much as 53 percent with an average deviation of 40 percent. The only experimental specific heat data available for the compressed liquid region below 110 K were those of van Itterbeek et al. [9]. The agreement between these data and values calculated from the equation of state was poor, the average deviation being about 15 percent, in C_v and 5 percent in C_p. However, these experimental data appear to have some internal inconsistency, and it is difficult to assess their reliability. Unfortunately no other experimental data exist in this region, leaving it somewhat in doubt. Good agreement was obtained between the calculated specific heats and the experimental data of Lestz [55]. These data were taken at temperatures of 273.15 and 303.7 K at pressures to 12 atm. The maximum deviation between calculated values and these data for both C_p and C_v is 0.37 percent. The data of Michels et al. [47] and Michels et al. [48] cover a temperature range from 133.15 to 423.15 K with pressures to 2423 atm. Excluding the critical region and the compressed liquid where deviations ranged to 9

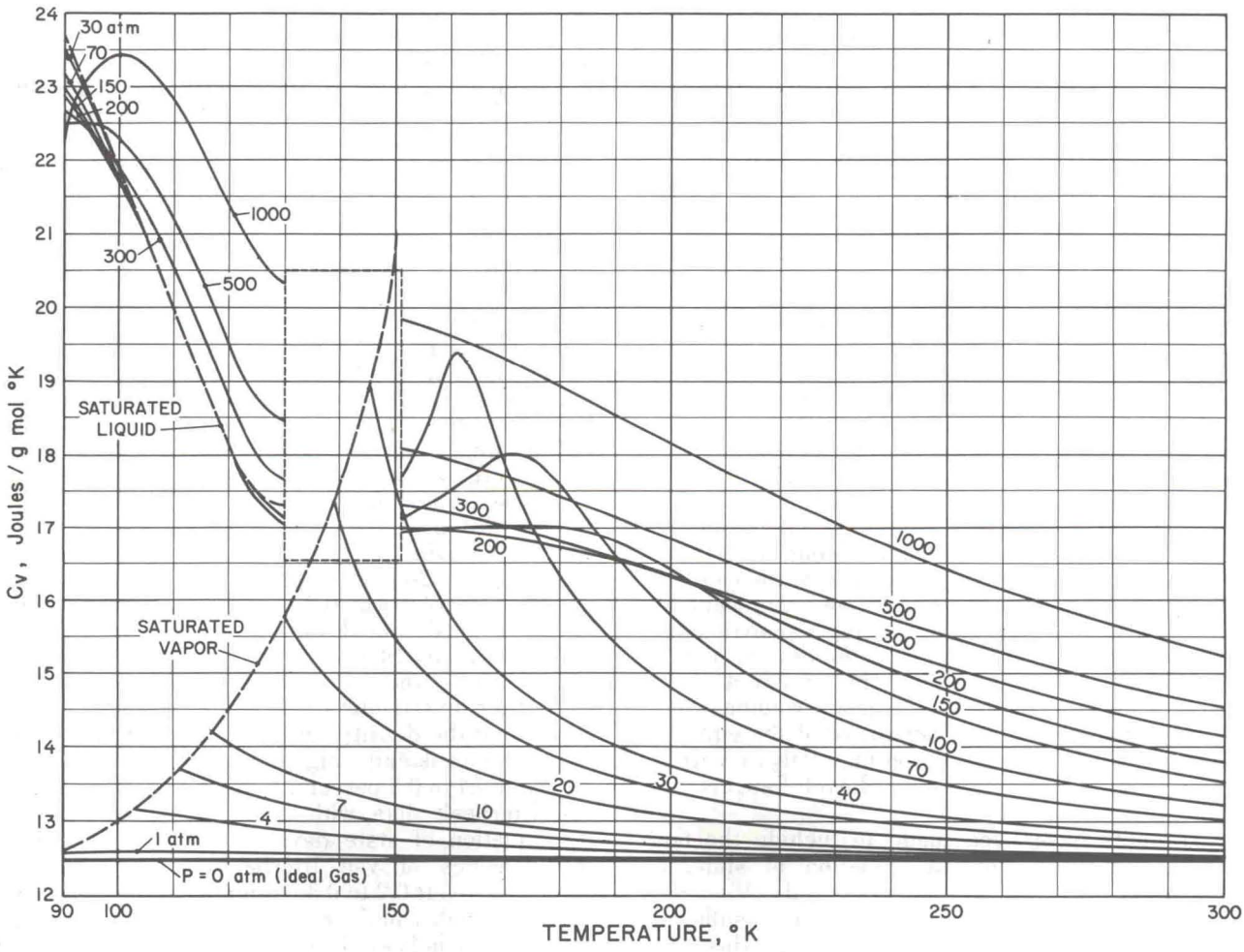

FIGURE 22. *Specific heat at constant volume calculated by numerical method.*

percent, the maximum deviation between experimental and calculated C_v's was 6.4 percent at 2423 atm and 398.15 K. The maximum C_p deviation for this group of data was 5.8 percent at 163.15 K and 70 atm. The specific heat data of Walker [11] were also compared with values calculated from the equation of state. The agreement between these data and the calculated values was slightly worse than the agreement obtained with Michels' data. However, the reliability of these data is believed to be less than that of Michels.

Comparison of the specific heats calculated here and those tabulated by two other correlations revealed satisfactory agreement. The C_p's tabulated by Hilsenrath et al. [27] for temperatures of 240 K and above agree with the values calculated here to better than one percent. However, the C_p's tabulated by Hilsenrath et al. [27] for temperatures below 240 K do not agree as well, especially at the high pressures. For example, at 200 K and 100 atm, the disagreement is about 10 percent in C_p while the value tabulated by Din [31] for this temperature and pressure agrees with this report to within 1.5 percent. The average deviation in C_p between this report and Din [31] is about 1.5 percent, which is much greater than the average deviation between this report and Hilsenrath et al. [27].

It is difficult to formulate a single equation of state which predicts valid *P-V-T* values over the liquid, vapor and critical point regions, and which also permits accurate calculation of specific heats. The specific heat of a fluid is a function of the second derivative of the equation of state. As pointed out in section 8, slight systematic deviations between the experimental *P-V-T* surface and the equation of state become magnified when derivatives are taken. The effect of these deviations becomes greater as higher order derivatives are taken and, in the region of the critical point where the equation of state has the largest systematic deviations, the second order derivatives contribute large errors to the specific heats.

15. Conclusions

An equation of state has been developed which represents the experimental *P-V-T* data for both the liquid and vapor phases, with a consistent transition from the low temperature-high density region to the low density region. Since some of multiple data sources are inconsistent where they overlap, it is difficult to assign an overall "figure of merit" for the adequacy of the equation of state as compared to an experimental *P-V-T* surface. In general, the equation of state represents the different sources of experimental data to within the accuracy of the data except in the region of the critical point. Numerous deviation plots have been presented so that direct comparisons between the equation of state and each source of experimental data can be made.

In the region of the critical point, the equation of state has a mean density deviation of about one percent and shows a systematic trend which can be attributed to the form of the equation of state. The critical point region has isotherms which undergo large changes in their first and second derivatives. Therefore, it is difficult to represent this critical point region and, at the same time, represent the liquid and vapor regions with a single analytic equation of state. The difficulty near the critical point is magnified when considering the apparent divergence of the specific heat at constant volume (which is related to the second derivative of the equation of state) which was found experimentally by Voronel et al. [54] and discussed by Levelt-Sengers and Vicentini-Missoni [56].

Attempts have been made to include the nonanalytic character of the equation of state, as discussed by Levelt-Sengers and Vicentini-Missoni [56]. However, at the present, insufficient progress has been made in including this nonanalytic behavior in equations of state which are explicit in pressure or density and cover a large range of the *P-V-T* surface.

Recent comments by Heller [57] and Pings and Teague [58] indicate that the critical temperature (and hence the critical pressure) stated earlier in this work may be slightly in error. However, definitive experimental verification of these comments is not yet available and the values for the critical temperature and pressure stated in this work appear to be the best estimate which is available at this writing.

Since the development of the equation of state, some new data on the *P-V-T* measurements of liquid argon have been published by van Witzenburg and Stryland [59]. These data cover the region from about 95 to 150 K at pressures from about 100 to 1900 atm. A comparison was made between these data and the values of density predicted by the equation of state. For the 38 points at 115 K and below, the mean density deviation was 0.15 percent, with one point having a maximum deviation of 0.5 percent. For the 126 points from 120 to 150 K, the mean density deviation was 0.3 percent with three points having a maximum deviation of 0.5 percent. Van Witzenburg and Stryland state that there were two small regions where their data could be compared with other investigators. One of these comparisons shows that the density values of van Itterbeek et al. [9] were consistently higher than van Witzenburg by about 0.4 to 0.5 percent. Comparison of the same van Itterbeek data with the values predicted by the equation of state developed here shows that the densities of van Itterbeek are consistently higher by about 0.2 to 0.3 percent. The second comparison which could be made shows that six data points of Michels et al. [1] had densities which were about 0.25 percent lower than van Witzenburg.

Comparison of the same six points of Michels with the values predicted by the equation of state developed here shows a mean density deviation of 0.03 percent.

An abundance of thermodynamic data for argon is available in the literature. However, it is only quite recent that investigators have begun to appreciate the inherent difficulties associated with obtaining good data in the region of the critical point. New techniques are being utilized to investigate critical point behavior, and older techniques are being updated to include the high precision which is necessary to describe this region. Theoretical studies are being made to try to understand the behavior in this interesting region. But much more experimental and theoretical work has yet to be done before a complete and definitive description of this critical region can be obtained.

16. Acknowledgements

The principal support for this work was furnished by the National Aeronautics and Space Administration, Office of Advanced Research and Technology, Contract R–06–006–046.

We wish to acknowledge the Mechanical Engineering Department of the University of Iowa, where this work began as a dissertation. In particular, we would like to acknowledge the guidance and assistance of J. Merle Trummel, of the University of Iowa, who served as academic advisor to the first author.

We are also grateful to R. B. Stewart, presently at Worcester Polytechnic Institute, for his comments and valuable suggestions during the initial phases of this work.

The authors also take pleasure in acknowledging the help of N. A. Olien, L. A. Hall, and the staff of the Cryogenic Data Center of the National Bureau of Standards at Boulder, Colo., who offered their valuable assistance in conducting an exhaustive literature search.

316-977 O - 69 - 3

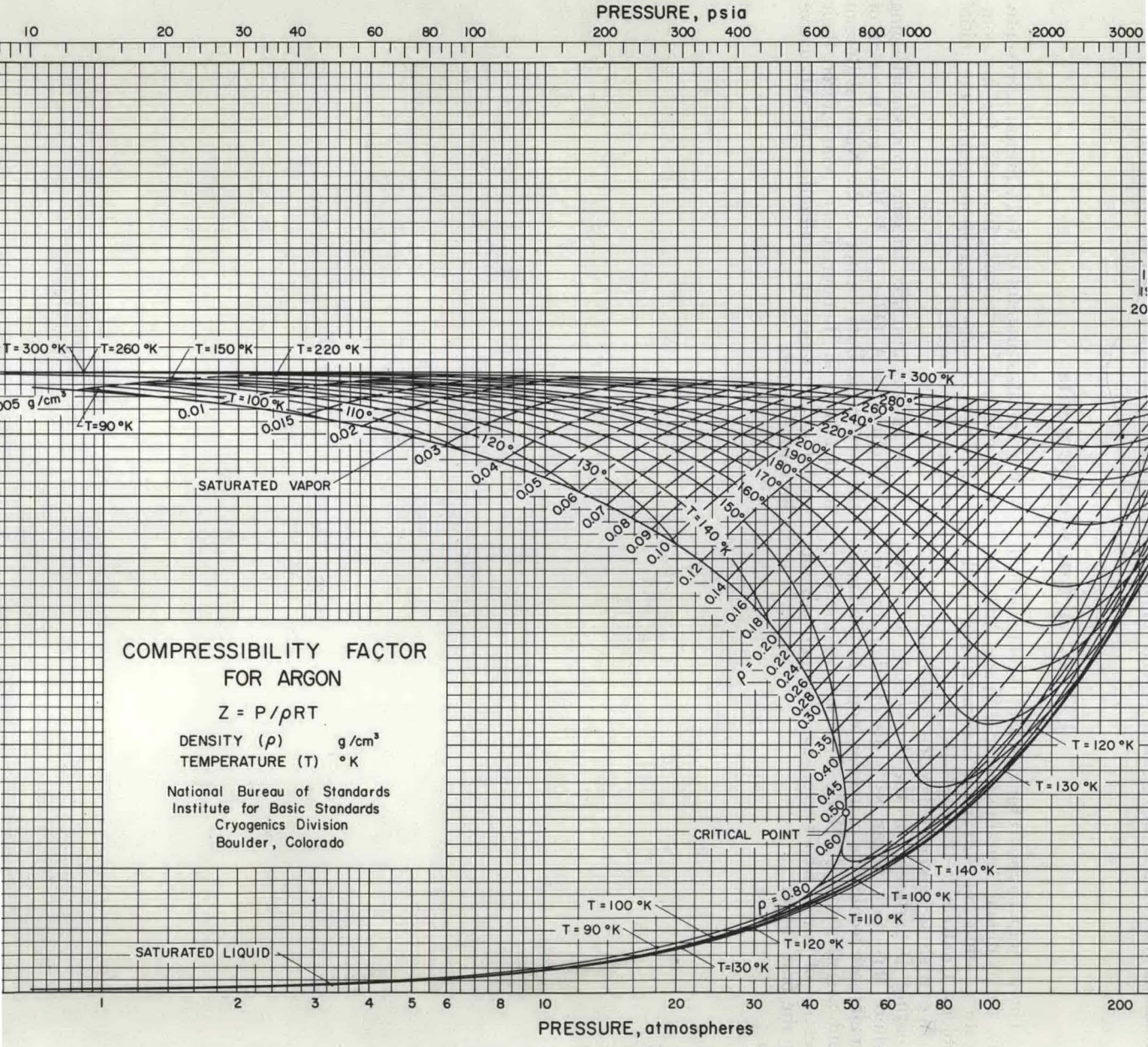

FIGURE 23. *Compressibility factor chart.*

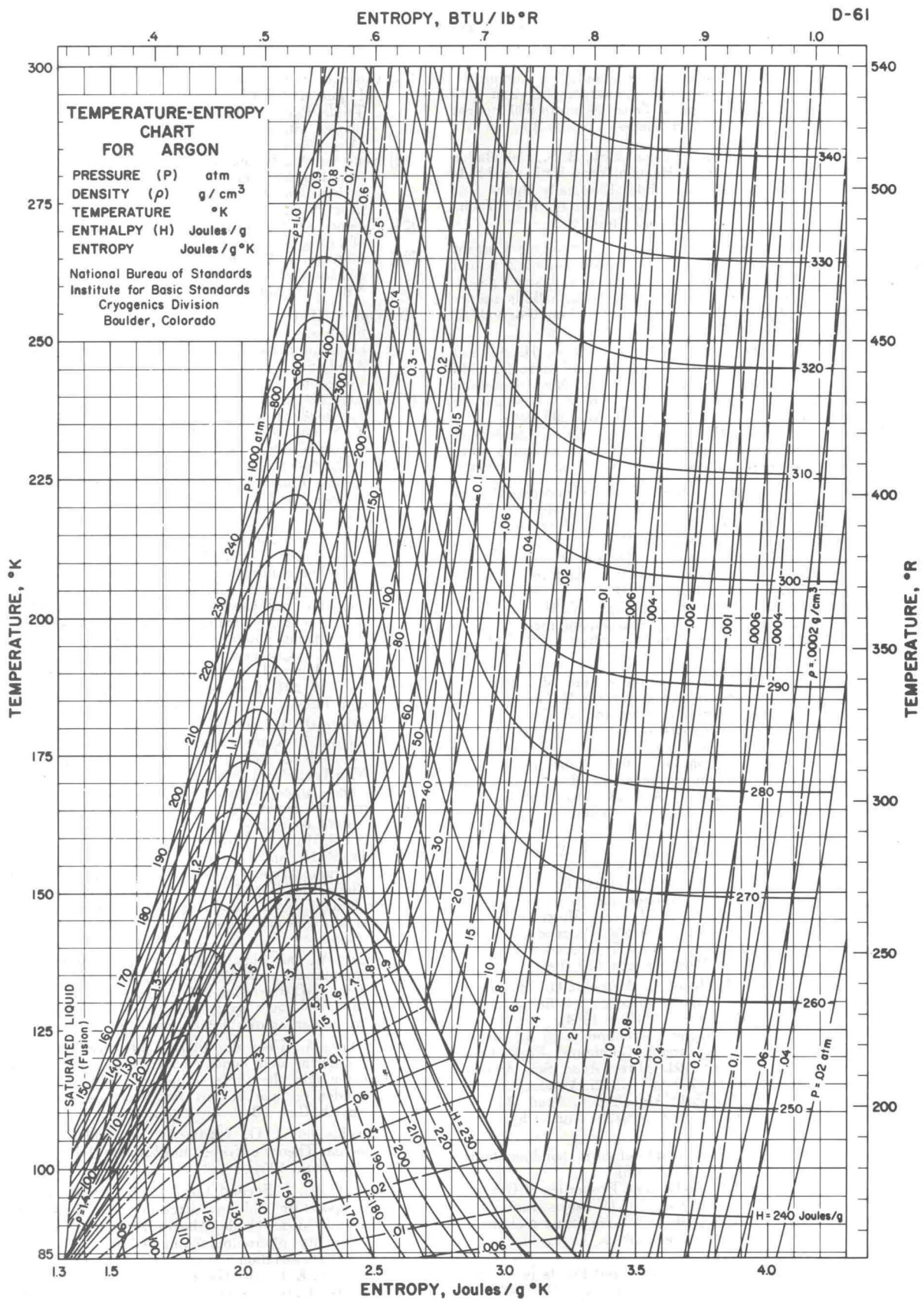

FIGURE 24. *Temperature-entropy chart.*

17. References

[1] Michels, A., Levelt, J. M., and de Graaff, W., Compressibility isotherms of argon at temperatures between −25 and −155 degrees C and at densities up to 640 amagat (pressures up to 1050 atmospheres), Physica **24,** 659–671 (1958).

[2] Ziegler, W. T., Mullins, J. C., and Kirk, B. S., Calculation of the Vapor Pressure and Heats of Vaporization and Sublimation of Liquids and Solids, Especially Below One Atmosphere Pressure. II. Argon, Georgia Inst. Tech., Eng. Exp. Sta., Tech. Rept. No. 2 (June 1962).

[3] Bureau of the Census, U.S. Dept. of Commerce Current Industrial Reports 1928A(65)−13 supplement 2 issued Jan. 20, 1967 for 1965 production of Industrial gases.

[4] Hall, L. A., Hust, J. G., and Gosman, A. L., A Bibliography of Thermophysical Properties of Argon from 0 to 300 °K, NBS Tech. Note 217 (June 1964).

[5] Hirschfelder, J. O., Buehler, R. J., McGee, H. A., and Sutton, J. R., A generalized equation of state for both gases and liquids. I., Wisconsin, Univ. Naval Research Lab., Dept. of Chemistry, Tech. Rept., Wis−Oor−15 (Oct. 5, 1956) Ind. Eng. Chem. **50,** 375–385, 1958.

[6] Michels, A., Wijker, H., and Wijker, H. K., Isotherms of argon between 0 and 150 degrees C and pressures up to 2900 atmospheres, Physica **15,** No. 7, 627–633 (1949).

[7] Rogovaya, I. A., and Kaganer, M. G., Compressibility of argon at low temperatures up to 200 atmospheres, Russ. J. Phys. Chem. **35,** 1049–1050 (1961) (English translation), Zhur. Fiz. Khim. **35,** 2135–2136 (1961).

[8] van Itterbeek, A., and Verbeke, O., Density of liquid nitrogen and argon as a function of pressure and temperature, Physica **26,** No. 11, 931–938 (1960).

[9] van Itterbeek, A., Verbeke, O., and Staes, K., Measurements on the equation of state of liquid argon and methane up to 300 kg/sq cm at low temperatures, Physica **29,** 742–754 (1963).

[10] van Witzenburg, W., The Equation of State of Liquid and Solid Argon, Toronto Univ., Canada, Ph. D. Thesis (1963).

[11] Walker, P. A., The Equation of State and the Specific Heat of Liquid Argon, University of London, Ph. D. Thesis (1956).

[12] Private communication from O. Verbeke, Laboratorium voor Lage temperaturen, Leuven, Belgium (1965).

[13] Private communication from P. A. Walker, Research Laboratories, General Electric Co., Ltd., Wembley, Middlesex, England (1961).

[14] Clark, A. M., Din, F., Robb, J., Michels, A., Wassenaar, T., and Zwietering, Th., The vapour pressure of argon, Physica **17,** No. 10, 876–884 (1951). 116th publication of the van der Waals Fund, Amsterdam, Nederland.

[15] Flubacher, P., Leadbetter, A. J., and Morrison, J. A., Thermodynamic Properties of Argon, Proceedings of the International Conference on Low Temperature Physics, 7th, Toronto, Canada, 1960, pp. 695–697 (1961).

[16] van Itterbeek, A., de Boelpaep, J., Verbeke, O., Theeuwes, F., and Staes, K., Vapour pressure of liquid argon, Physics **30,** No. 12, 2119–2122 (Dec. 1964).

[17] Mathias, E., Onnes, H. K., and Crommelin, C. A., On the rectilinear diameter for argon, Communs. Phys. Lab., Univ. Leiden, No. 131A (1912), Proc. Acad. Sci., Amsterdam **15,** 667–673 and 960–965 (1912); Verslag Gewone Vergader Wis- En Natuurk. Afdeel. Kon. Akad. Wetenschap, 700–706 and 893–898 (1912); Ann. Phys. **17,** 442–455 (1922).

[18] Guggenheim, E. A., The principle of corresponding states, J. Chem. Phys. **13,** 253–261 (1945).

[19] Stewart, R. B., The Thermodynamic Properties of Oxygen, State Univ. of Iowa, Iowa City, Ph. D. Thesis (June 1966).

[20] Hust, J. G., and McCarty, R. D., Curve-fitting techniques and applications to thermodynamics, Cryogenics **7, 4,** 200–206 (Aug. 1967).

[21] Hoge, H. J., Vapor Pressure and Fixed Points of Oxygen and Heat Capacity in the Critical Region, J. Res. NBS **44,** 321–345 (1950) RP2081.

[22] Gosman, A. L., Thermodynamic Properties of Argon in the Liquid and Gaseous State for Temperatures From the Triple Point to 300 °K With Pressures to 1000 Atmospheres, State Univ. of Iowa, Iowa City, Ph. D. Thesis (Aug. 1965).

[23] Benedict, M., Webb, G. B., and Rubin, L. C., An empirical equation for thermodynamic properties of light hydrocarbons and their mixtures, J. Chem. Phys. **8,** 334–345 (Apr. 1940).

[24] Bloomer, O. T., and Rao, X. N., Thermodynamic properties of nitrogen, Inst. Gas Tech. Res. Bull. **18** (Oct. 1952).

[25] Strobridge, T. R., The Thermodynamic Properties of Nitrogen from 64 to 300 °K between 0.1 and 200 Atmospheres, NBS Tech. Note No. 129, PB 161630 (1962).

[26] Onnes, H. K., and Crommelin, C. A., Isotherms of monatomic gases and of their binary mixtures. VII. Isotherms of argon between 20 degrees and −150 degrees, Proc. Acad. Sci. Amsterdam **13,** 614–625 (1911) reprinted in Communs. Phys. Lab. Univ. Leiden No. 118b (1911).

[27] Hilsenrath, J., Beckett, C. W., Benedict, W. S., Fano, L., Hoge, H. J. Masi, J. F., Nuttall, R. L., Touloukian, Y. S., and Woolley, H. W., Tables of Thermal Properties of Gases, NBS Circ. No. 564 (1955), reprinted as Tables of Thermodynamic and Transport Properties of Air, Argon, Carbon Dioxide, Carbon Monoxide, Hydrogen, Nitrogen, Oxygen, and Steam (Pergamon Press, Oxford, 1960) 478 pp.

[28] Private communication from J. M. H. Levelt-Sengers, National Bureau of Standards, Gaithersburg, Md (1964).

[29] Private communication from C. R. Barber, National Physical Laboratory, Teddington, Middlesex, England (1967).

[30] Hust, J. G., and Gosman, A. L., Functions for the calculation of entropy, enthalpy, and internal energy for real fluids using equations of state and specific heats, Advances in Cryogenic Engineering **9,** 227–233 (1964).

[31] Din, F., Argon, Thermodynamic Functions of Gases, Vol. **2,** pp. 146–201 (Butterworths Scientific Publications, London, 1956).

[32] Goodwin, R. D., and Weber, L. A., A Comparison of Two Melting-Pressure Equations Constrained to the Triple Point Using Data for Eleven Gases and Three Metals, NBS Tech. Note 183 (Oct. 1963).

[33] Michels, A., and Prins, C., The melting lines of argon, krypton and xenon up to 1500 atm; representation of the results by a low of corresponding states, Physica **28,** No. 2, 101–116 (Feb. 1962).

[34] Lahr, P. H., and Eversole, W. G., Compression isotherms of argon, krypton, and xenon through the freezing zone, Chem. Eng. Data **7,** No. 1, 42–47 (Jan. 1962).

[35] Bridgman, P. W., The melting curves and compressibilities of nitrogen and argon, Proc. Am. Acad. Arts Sci. **70,** 1 (1935).

[36] Frank, A., and Clusius, K., Prazisionsmessungen der Verdampfungswarme Der Gase O_2, H_2S, PH_3, A, COS, CH_4, and CH_3D (Precision measurements of the heat of vaporization of gases oxygen, hydrogen sulphide, phosphene, argon, carbon oxisulphide, methane and deuteromethane)

[37] Eucken, A., Uber das thermische verhalten einiger komprimierter und kondonsierter gase bei tiefen temperaturen (On the thermal behavior of a compressed and condensed gas at low temperatures) Verhandl. Deut. Physik. Ges. **18,** 4–27 (1916).

[38] Hirschfelder, J. O., Curtiss, C. F., and Bird, R. B., Molecular Theory of Gases and Liquids (John Wiley & Sons, New York, 1954).

[39] Kerr, E. C., I. Second Virial Coefficient of Argon at Low Temperature and Low Pressure., II. Heat Capacity of Liquid Nitric Oxide Above its Normal Boiling Point., University Microfilms (Ann Arbor, Mich.), Publ. No. 21480, Dissertation Abstracts **17,** 1232 (1957).

[40] Fender, B. E. F., and Halsey, G. D., Jr., Second virial coefficients of argon, krypton, and argon-krypton mixtures at low temperatures, J. Chem. Phys. **36,** 1881–1888 (1962).

[41] Holborn, L., and Otto, J., Uber die isothermen einiger gase zwischen 400 und −183 grad. (On the isotherms of various gases between 400 and −183 degrees C.), Z. Physik **33,** 1–11 (1925).
[42] Hanley, H. J. M., Comparison of the Lennard-Jones, Exp: 6 and Kihara potential functions using viscosity data of dilute argon, J. Chem. Phys. **44,** 4219 (1966).
[43] Private communication from M. Klein, National Bureau of Standards, Gaithersburg, Md. (1967).
[44] Hanley, H. J. M., and Klein, M., On the selection of the intermolecular potential function: application of the statistical mechanical theory to experiment, NBS Tech. Note No. 360 (Nov. 1967).
Hanley, H. J. M., and Klein, M. On the selection of the intermolecular potential function: Part 2, from pair properties, Trans. Faraday Soc. (in press).
[45] Roebuck, J. R., and Osterberg, H., The Joule-Thomson effect in argon, Phys. Rev. **46,** 785–790 (1934).
[46] Roebuck, J. R., and Osterberg, H., The Joule-Thomson effect in mixtures of helium and argon, J. Chem. Phys. **8,** 627–635 (1940).
[47] Michels, A., Levelt, J. M., and Wolkers, G. J., Thermodynamic properties of argon at temperatures between 0 and −140 degrees C and at densities up to 640 amagat (pressures up to 1050 atmospheres.), Physica **24,** 769–794 (1958).
[48] Michels, A., Lunbeck, R. J., and Wolkers, G. J., Thermodynamical properties of argon as function of density and and temperature between 0 and 150 degrees C and densities to 640 amagat, Physica **15,** 689–695 (1949).
[49] Weir, R. D., Jones, I. W., Rowlinson, J. S., and Saville, G., Equation of state of gases at low temperatures. Part 1. Second virial coefficients of argon and krypton., Trans. Faraday Soc. **63,** No. 534, 1320–1329 (1967).
[50] Holborn, L., and Otto, J., The isotherms of several gases up to 400 degrees and their importance for the gas thermometer, Z. Phys. **23,** 77–94 (1924).
[51] Holborn, L., and Otto., J., Isotherms for helium, nitrogen, and argon below 0 degrees C, Z. Phys. **30,** 320–328 (1924).
[52] Holborn, L., and Schultze, H., Uber die Druckwage und die Isothermen von Luft, Argon und Helium Zwischen 0 und 200 Degrees. (Concerning the pressure scale and the isotherms of air, argon, and helium between 0 and 200 Degrees), Ann. Phys. **47,** 1089–1111 (1915).
[53] van Itterbeek, A., and van Paemel, O., Measurements on the velocity of sound in gaseous argon and deuterium respectively at liquid oxygen and hydrogen temperatures. Calculation and discussion of the second virial coefficient of argon, Physica **5,** 845–853 (1938).
[54] Voronel, A. V., Snigirev, V. G., and Chashkin, Yu. R., Behavior of the specific heat C_v of pure substances near the critical point, Sov. Phys. JETP **21,** No. 3, 653–655 (Sept. 1965); Trans. of Zh. Eksp. Teor. Fiz. **48,** 981–984 (Mar. 1965).
[55] Lestz, S. S., Acoustic isotherms for nitrogen, argon, and krypton, J. Chem. Phys. **38,** 2830–2834 (1963).
[56] Sengers, J. M. H. L., and Vicentini-Missoni, M., Thermodynamic Anomalies near the Gas-liquid Critical Point, Proceedings of the Fourth Symposium on Thermophysical Properties, pp. 79–86 (1968).
[57] Heller, P., Experimental investigations of critical phenomena, Repts. Progr. Phys. **30,** Pt. 2, 731–826 (1967).
[58] Pings, C. J., and Teague, R. K., Experimental study of the shape of the coexistence curve of argon near the critical state, Phys. Letters **26A,** No. 10, 496–497 (Apr. 1968).
[59] van Witzenburg, W., and Stryland, J. C., Density measurements of compressed solid and liquid argon, Can. J. Phys. **46,** 811–816 (1968).